Title

The subtropical global plume in the Pacific Exploratory Mission-Tropics A (PEM-Tropics A), PEM-Tropics B, and the Global Atmospheric Sampling Program (GASP): How tropical emissions affect the remote Pacific

Authors

Chatfield, RB
Guo, Z
Sachse, GW
et al.

Peer reviewed

The subtropical global plume in the Pacific Exploratory Mission-Tropics A (PEM-Tropics A), PEM-Tropics B, and the Global Atmospheric Sampling Program (GASP): How tropical emissions affect the remote Pacific

R. B. Chatfield and Z. Guo[1]

NASA Ames Research Center, Moffett Field, California, USA

G. W. Sachse

NASA Langley Research Center, Virginia, USA

D. R. Blake and N. J. Blake

University of California, Irvine, California, USA

[1] An extended southern subtropical plume of CO meanders >15,000 km around the world, gradually spreading around ~20 S. This southern pollution plume is most noticeable in the burning season, southern spring; a similar subtropical plume appears in the northern spring. We use tracer maps to guide the use of trajectories to trace observations of the plume to their origins. The MM5 mesoscale model provides high-resolution, near-global synoptic reconstructions of the weather. Two situations are analyzed: NASA's airborne Pacific Exploratory Mission-Tropics A (PEM-Tropics A) period, September–October 1996 and the PEM-Tropics B period, March–April 1999. Similar features are noted for a much earlier mission in 1977, which apparently captured the first, but never-recognized, samples of the global pollution of the Southern Hemisphere. For PEM-Tropics A, near-source pieces of the plume are clearly seen in the Total Ozone Mapping Spectrometer (TOMS) absorbing aerosol product and are well simulated. Downwind, the aircraft sampling of several strands deriving from a single plume seems representative and well simulated. A general mechanism of the plume emerges: The southern plume arises in surface accumulation regions in Africa and South America. Thunderstorm-scale venting of pollutants usually lofts the plume; however, synoptic-scale lifting can produce intense outbreaks. The plume flows eastward in the subtropical jet region as a single coherent but articulated current until it is increasingly filamented by storms in the Pacific. A similar northern subtropical plume is described for the PEM-Tropics B period. The 100-km model resolution we used seemed to capture much of the variability. However, the model somewhat under predicted the highest values.   INDEX TERMS: 3319 Meteorology and Atmospheric Dynamics: General circulation; 0345 Atmospheric Composition and Structure: Pollution—urban and regional (0305); 0322 Atmospheric Composition and Structure: Constituent sources and sinks; 9355 Information Related to Geographic Region: Pacific Ocean; 1610 Global Change: Atmosphere (0315, 0325); KEYWORDS: global pollution, subtropical jet, long-distance transport, biomass burning, pristine atmosphere, cloud venting

1. Introduction

[2] The Pacific Exploratory Mission-Tropics A (PEM-Tropics A) was planned mainly as an opportunity to sample the clean atmosphere. This mission has been described by *Hoell et al.* [1999], and remarks about the numerous

pollution layers discovered are reported by *Fuelberg et al.* [1999], *Schultz et al.* [1999], *Staudt et al.* [2001], and A. Staudt et al., Sources and chemistry of nitrogen oxides over the tropical Pacific, submitted to *Journal of Geophysical Research,* 2002, hereinafter referred to as Staudt et al., submitted manuscript, 2002). Schultz's Figure 2 shows the wide survey of the South Pacific Ocean that was made in the survey aboard NASA's DC-8 flying laboratory. Although substantial pollution was long known to occur in the Southern Hemisphere [*Selier and Crutzen*, 1980], it was presumed to be concentrated mainly in the South

---

[1]Now at WNI Oceanroutes, Sunnyvale, California, USA.

Tropical Atlantic and the adjoining continents. There was considerable surprise when the DC-8 aircraft measurements repeatedly reported plumes of pollution, evidently from biomass burning. A return sampling expedition, PEM-Tropics B in spring 1999, found much less pollution in the Southern Hemisphere; our work will show that the DC-8 and P-3 might have sampled a similar phenomenon in the Northern Hemisphere.

[3] In both expeditions, NASA's P-3 aircraft also sampled biomass-burning plumes, predominantly from northern South America, relatively nearby. While this plume is clearly evident in our results, detailed description of these equatorial plumes, with restricted reach, is a topic for a future paper. Our description of a "Great African Plume" from equatorial Africa [*Chatfield et al.*, 1998] provided one example. From the viewpoint of the current paper we would say that Africa feeds both an equatorial plume (∼3000 km) and a subtropical global plume (∼20,000 km). The equatorial plume is responsible for most of the pollution buildup noted in the Atlantic. When the Pacific plumes were discovered in PEM-T A, questions immediately arose: (1) How typical was the sampling along the chosen DC-8 flight paths? (2) If the sampled pollutants were signals of biomass burning, where did they come from and how did they get to the mid-Pacific so undilute? (3) To what extent were the plumes a feature of just one exotic month during the year, or to what extent did they describe a broader seasonal pattern of continental influence of the remote oceanic troposphere? To the extent the plumes do modify a significant amount of the Pacific large-scale chemistry, there is a fourth question: (4) What resolution and detail in parameterizations and algorithms are necessary to represent tropospheric traces species accurately in the simulation of global pollution chemistry and the developing effects on climate?

1.1. The Pristine Remote South Pacific: Missing the Lessons of the Global Atmospheric Sampling Program (GASP)

[4] The occasionally relatively polluted nature of the South Pacific had been discovered long before PEM-Tropics A, but the evidence apparently had been ignored, perhaps because contamination had seemed so improbable. This section outlines our understanding of the "pristine South Pacific atmosphere" and these earliest contradicting measurements. For decades the troposphere of the South Pacific has been viewed as a preserve of reliably pristine air, and for most of Earth the upper troposphere has been considered cleaner than the surface layers. *Selier*'s [1974] two-dimensional description of the cycle of atmospheric CO provided a general picture for modelers for the next 15 years: Anthropogenic pollution, especially from combustion, spread out from the Northern Hemisphere's industrialized continents. Interhemispheric transport of this CO to the subtropical upper troposphere was thought to cause an inversion of CO. Models of tropospheric chemistry [e.g., *Logan et al.*, 1981; *Crutzen and Gidel*, 1983] were, in part, judged by their faithfulness in reproducing a picture of a polluted Northern Hemisphere (considered largely continental) and a clean (oceanic) Southern Hemisphere.

[5] These models were based on a view of the tropospheric circulation as largely zonally symmetric, a view that continues to be relevant in the stratosphere. In the one- and two-

dimensional models employed, diffusion carried out most of the transport. This view continued even to the early modern generation of three-dimensional (3-D) models [*Crutzen and Zimmermann*, 1991; *Brasseur et al.*, 1996], which depended on monthly average winds and diffusion coefficients. Experimental evidence near the surface, especially outside the tropics, corroborated this view of rapidly diffusing plumes of pollutants. Once plumes moved out to the synoptic scale, they dispersed in the characteristic turning and shearing motions of midlatitude anticyclones and cyclonic storms. Surveys of the Pacific troposphere in various seasons, e.g., the ambitious Global Atmospheric Measurements of Trace Aerosols and Gases (GAMETAG), seemed to confirm these ideas [e.g., *Heidt et al.*, 1980]. The picture of a clean atmosphere above tropical oceans began to break down with the discovery of high ozone flowing in from the South Atlantic [*Logan and Kirchoff*, 1986; *Fishman et al.*, 1991]. Still, on the basis of both models and measurements, pollution of the troposphere seemed primarily restricted to the source regions near the Greenwich meridian.

[6] A certain amount of evidence pointed to the contrary, and so we will make a digression about a prolonged period of missed opportunity to learn from the data. The Global Atmospheric Sampling Program made measurements at near-tropopause flight altitudes on an around-the world mission in late October 1977. Relatively little variation between 0° and 180° longitudinal transects in the southern tropics and subtropics were noted (89 versus 66 ppb). The southern Pacific was found to have the same or more CO than the Pacific north of the Intertropical Convergence Zone (ITCZ) [*Pratt and Falconer*, 1979]. What seem now to be clear plumes of CO were shown (>90 ppb CO at 27°S, >80 ppb at 33°S, and ∼80 ppb at 15°S). However, the instrument's detection and accuracy were limited (quoted as 20 ppb and 12%). Furthermore, drift compromised the instrument [*Pratt and Falconer*, 1979]. The resulting uncertainty may have limited the need to reconsider then-current theory. Consequently, there was not much reevaluation of the "pristine remote oceanic Pacific" concept. In hindsight the results look flawed but informative. There were satellite measurements such as the Measurement of Air Pollution from Space (MAPS) in 1984, which did suggest puzzling high values of column CO far from the source region, but again, the sampling had difficulties. The sampled region beneath the space shuttle was very narrow, the sampling duration was brief, and there was a period of reanalysis of the primary radiance data. The limitation of the measurements to those that could be viewed at the nadir during a manned spacecraft mission of a few days meant that the pattern of coverage made interpretation difficult. *Pougatchev et al.* [1999] have recently put these MAPS data and the PEM-Tropics A data into an historical perspective.

1.2. Prior Modeling of Biomass-Burning CO

[7] It appears worthwhile to make a brief summary of a long history of the simulation of atmospheric CO. Three-dimensional modeling of CO began quite early. For example, *Kwok et al.* [1971] treated CO as an inert tracer within a general circulation model. Early work treated the urban pollution and methane sources of carbon monoxide, and we will not attempt to survey all efforts. *Peters and Jouvanis* [1979] pioneered in using observed meteorology to drive

simulations. *Pinto et al.* [1983] found that a very large source of CO in equatorial latitudes was necessary to explain tropical CO observations. Chatfield initially wrote that the oxidation of isoprene and similar organics from trees also provided a broadly distributed source, though it was one that was particularly difficult to quantify [*Zimmerman et al.*, 1978]. The concentrated source proved to be predominantly biomass burning [*Crutzen et al.*, 1979]. The interannual variation of CO mixing ratios observed at scattered surface sites has served to focus interest on the role of CO in controlling the general level of tropospheric hydroxyl radical. *Granier et al.* [1996] summarize recent work on the chemistry and biogeochemistry of interannual variation of CO. *Galanter et al.* [2000] have used CO analyses in describing broader biomass-burning effects on the global atmosphere, and their work helps explain our motivation to focus on meteorology and events. Staudt et al. (submitted manuscript, 2002) similarly consider full-chemistry simulations at coarser resolution and reinforce our description of CO as a premier tracer. *Allen et al.* [1996] have focused on the role of interannual transport variations. *Holloway et al.* [2000] make comparisons of several sources with a broader-brush approach. *Allen et al.* [1996] very clearly show a large southern global plume of carbon monoxide, but previous works do not concentrate on meteorology of its origin, nor do they make extensive comparisons to remote free-tropospheric observations. That is the focus of this paper.

1.3. Outline and General Thesis

[8] In this paper, we bring together strands of previous descriptions to provide a more unified picture of the southern global plume. The model used was not able to describe completely the processes determining CO, and that is not our intention. Rather, it is a high-resolution model available to us which seems adequate to describe some general principles that help explain what is lacking in the "pristine oceanic troposphere" view and some general mechanisms of the pollution of the South Pacific. Different versions were prepared for PEM-Tropics A and PEM-Tropics B so as to capture the major quantitative effects for each situation. Clear indications that export of CO from South America and Africa would affect the Southern Ocean were visible in the mesoscale-synoptic model of *Chatfield et al.* [1998] and other work. Consequently, we used this available model at a greatly expanded domain, but finer resolution, to understand features of the global plume. In case studies we will illustrate a repeated pattern of events that lead to the southern global plume as measured in the remote Pacific: (1) a pattern of continental accumulation of pollutants; (2) a pattern of convergence and divergence associated with transport from the dry tropics; (3) a tendency toward intercontinental accumulation in the South Atlantic; (4) often, a supplemental injection of highly polluted material in a more complex flow as air crossed southern Africa, with additions occurring between 8 and 15 km; (5) a pattern of undulating but rapid undilute transport across the South Indian Ocean and Australia; (6) subsidence of the plumes by both isentropic and diabatic, radiative processes; (7) increasing undulation, splintering, and likelihood of dispersion as the plume moves into the Pacific Ocean, affected first by the South Pacific Convergence Zone (SPCZ) and finally by the

Andes. Wisps of plumes probably continue to circulate around the globe. These studies concentrate on plumes given some special attention by *Staudt et al.* [2001] and *Fuelberg et al.* [1999]. We will suggest that the individual processes associated with these plumes are typical of the transmission and eventual splintering of the southern global plume sampled in many instances, which are detailed in those papers.

[9] Following these studies, there will be shorter descriptions of attenuated subtropical plumes in the austral autumn and long ones in the boreal spring: a "northern global plume." Features of these plumes differ in appropriate ways.

[10] The discussion then turns to a statistical analysis and to some thoughts about the limitations of current simulation ability. This tracer analysis may have some implications for more complete models attempting to simulate the global tropospheric chemistry of ozone and oxidants [*Roelofs et al.*, 1997; *Hauglustaine et al.*, 1998].

2. Basic Methods

2.1. Mesoscale Model (MM5) Simulations

[11] When the PEM-Tropics A investigators reported pollutants in the South Pacific, we were motivated to help establish sources more conclusively. Our experience was not with global models but rather with the MM5 mesoscale/synoptic-scale model. We have used these to investigate the regional aspects of pollution lofting [*Chatfield et al.*, 1996, 1998]. The fifth-generation Pennsylvania State University/National Center for Atmospheric Research (NCAR) mesoscale model (MM5) was used to provide hourly weather conditions for this study. MM5 is a 3-D, map-projection primitive equation model with terrain-following sigma coordinates [*Grell et al.*, 1995]. We had some experience in using this model in what we believed to be a primary source region, Africa and South America [*Chatfield et al.*, 1998]. These simulations clearly indicated an export of concentrated pollutant plumes to the South Indian Ocean. We took the somewhat extreme step of running MM5 on a global scale. Since MM5 is run on a map projection, we chose the Mercator projection, our interest being on the subtropics and equatorial regions. A global wrap of the projection was easily accomplished by having very nearly duplicate grid points at 110°W. Since boundary conditions for MM5 are set at this boundary-wrap point [*Grell et al.*, 1995], we may expect slightly different behavior at this longitude; this may have degraded our precision, or at least meteorological self-consistency, near this meridian.

[12] The model simulation domain has 105 × 400 grid points and 23 sigma levels. The nominal grid size is 100 km, and the top layer is 70 hPa. The nonhydrostatic option of the MM5 version 2.11 was chosen, and the time step was 200 s. The initial and lateral boundary conditions were interpolated from 2.5 × 2.5 global objective analyses supplied by the European Centre for Medium-Range Weather Forecasts (ECMWF). These analyzed fields are also used for four-dimensional data assimilation (FDDA). An analysis-nudging FDDA approach is applied continuously to force the model simulated wind components (u, v), temperature (T), and water vapor mixing ratio (q_v) toward gridded analyses based on the observations. (FDDA combines observations and

model prognostic variables in the dynamical model and improves time continuity and dynamic coupling among the various fields.)

[13] In this study, explicit and implicit (parameterized) methods are employed to treat the resolved-scale rain and subgrid-scale convection, respectively. The MM5's hydrological cycle includes prognostic equations that are used to calculate q_v, cloud water, cloud ice, and rainwater. Seasonal values of water capacity for the soil are drawn from averages developed by *Potter et al.* [1993]. The Grell convective parameterization [*Grell*, 1993; *Grell et al.*, 1995] is used for the nonresolved convective motion. The information on hourly averaged cloud tops, cloud bases, heights of downdraft levels, strength of downdraft, and mass fluxes of clouds is output to a history file. In version 2.11 of MM5, as used, the precipitation efficiency is increased, and maximum downdraft is decreased by 10% to increase the effective upward motion in clouds.

[14] Other import features of the MM5 used in this study are the so-called Medium-Range Forecast (MRF) model [*Hong and Pan*, 1996] planetary boundary layer (PBL) model, and the Community Climate Model 2 (CCM2) radiative model. Turbulent fluxes of heat, moisture, and momentum are calculated within the PBL. The ground temperature is predicted from a surface energy budget equation that accounts for shortwave and longwave radiation, cloud cover, surface characteristics of albedo, roughness, thermal inertia, emissivity, and moisture availability.

2.2. The Global Regional Atmospheric Chemistry Event Simulator (GRACES) Model

[15] We employed our GRACES model, as described previously by *Chatfield et al.* [1996, 1998]. The record of winds, temperatures, surface pressures, boundary layer mixing heights, and Grell-scheme parameters from the MM5 history was used to feed the model, which integrates source parameterizations, transport, and transformation rates "off line" from the meteorological calculation. GRACES runs on essentially the same grid as MM5; Arakawa *B*-grid winds from MM5 are simply averaged for use on the GRACES Arakawa *C* grid [*Arakawa and Lamb*, 1977]. When the work was initiated, we used a modified version of the *Smolarkiewicz and Grabowski* [1990] transport scheme, exploiting a tuning of his *S* parameter and a nonoscillatory option, and the results of this scheme were used for most maps we present. We found better quantitative performance with a recently suggested scheme by *Walcek* [2000] on the basis of very local modification of a standard *van Leer* [1977] scheme around peaks. *Walcek* [2000] describes very good behavior in the numerical diffusion exhibited by his scheme (see his Figure 6) compared with most current schemes in the standard rotation problems. (We estimate that our version of the *Smolarkiewicz and Grabowski* [1990] transport scheme (coincidentally) approximated the behavior of the Bott L4 procedure in that figure.) The results of a computation with this algorithm were used for numerical comparisons.

[16] Cloud fluxes of carbon monoxide are extremely important in explaining CO distributions [*Pratt and Falconer*, 1979; *Dickerson et al.*, 1987; *Chatfield and Delany*, 1990], and correct mass-transport parameterizations are essential to estimates of the CO budget [*Chatfield et al.*,

1998]. Subgrid vertical transport of CO in cumulonimbus clouds is parameterized by using a single upward pipe and a single downward pipe, that is, entrainment of air in core updrafts and downdrafts is ignored [*Grell et al.*, 1995]. Our previous experience with the Transport and Atmospheric Chemistry near the Equator-Atlantic (TRACE-A) data suggested that this disregard of entrainment, or other causes, might have underestimated vertical transport although locations of convection appeared to be acceptably forecast. Additionally, we spread the detrainment of material at cloud top over the top three layers, with one-half at the cloud top the Grell scheme provides, one-third in the layer below, and the rest in the next layer down. These are very simple attempts to allow for some simple trends as the grid scale increases. It is fairly apparent that in doubling the horizontal grid spacing, four cloud tops must be represented by only one, and so spread-out detrainment (like that of *Arakawa and Schubert* [1974], often used for large-grid models) must be represented within the parameterization. It is less clear what the interaction of grid size and parameterization in determining mass flux may be. *Kuo et al.* [1995] describe the effect of coarser grid resolution on the behavior Grell scheme for a midlatitude case; in moving from 40- to 80-km resolution, precipitation in intense local storms could change by as much as a factor of 3. Precipitation is one measure of subgrid-scale vertical motion, as it is closely related to water vapor flux at parameterized cloud base. As is characteristic of such model problems, the locations of the intense features were not affected, and in some areas, precipitation was much less affected. Our simulations are at 110 km, and even larger effects of resolution may be conjectured. Conceivably, magnifications of cloud mass fluxes by even greater factors, or even different cumulonimbus parameterizations, are required. A significant difference in this work is that we did not multiply the cloud base mass transport reported from MM5 by a factor of 2.5, as we did in the earlier work, at a coarse 250-km resolution. Such an increase is consistent with the idea that the location and depth of convection may be accurately represented by a MM5 run that nevertheless underestimates moisture convergence (and therefore cloud mass flux) along the lines of the *Kuo et al.* [1995] analysis. Unpublished analyses suggest that perhaps a compensation factor of 1.25 might be more appropriate at the 100-km scale we employed.

[17] A last approximation made in GRACES is probably somewhat less significant than the approximation of cloud behavior. Carbon monoxide is treated as a passive tracer without chemical loss or production in the atmosphere. True, CO may have a lifetime of 20 days or less in the source regions near the surface of Earth, where both the OH radical and the pressure-dependent reaction rate coefficient are high. Two factors mitigate an apparent short-lifetime behavior. First, the lifetime is much longer in the upper troposphere and wherever water vapor is low. The observations made on the DC-8 show the air to be very dry. Thus, after the initial phase of photochemical activity caused by cumulonimbus venting of a smoggy biomass-burning mixture [*Chatfield et al.*, 1996], the OH-radical concentrations may well be depressed [*Schultz et al.*, 1999]. There are several other competing factors suggesting that we should either address a fairly complete CO chemistry or ignore it. CO is produced by methane in the free atmosphere to a
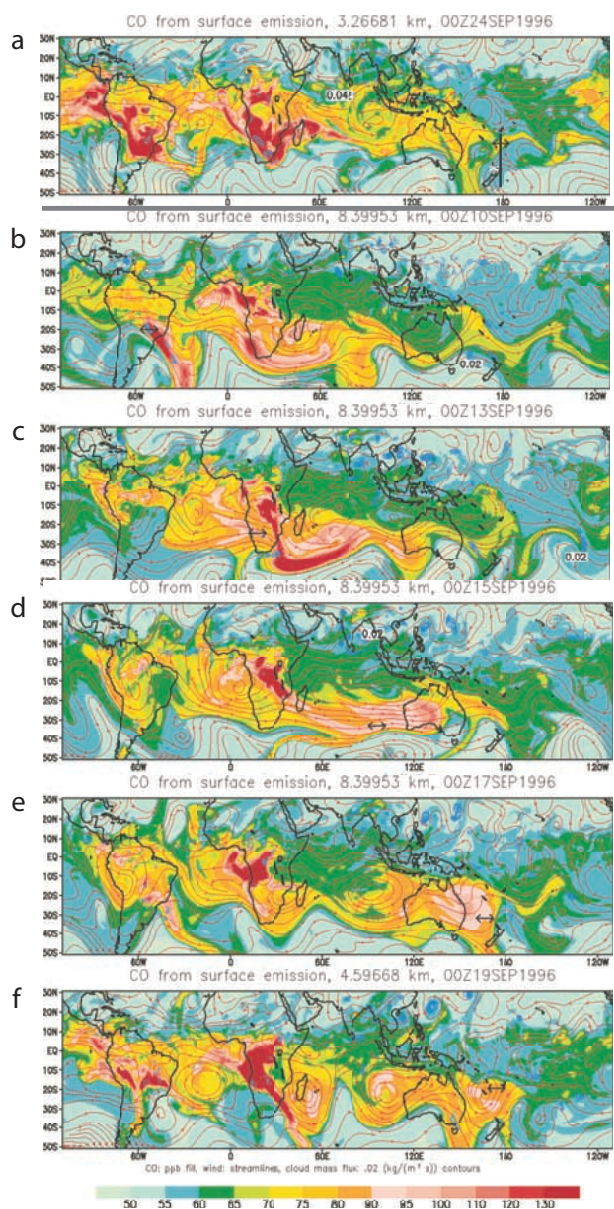
Figure 1. Map of the simulated spread of the southern global plume to the International Date Line region at 0000 UT on 24 September, approximately the same time of the observations shown in Figure 4. The north-south black line shows the sampling flight path, and the double-headed arrow shows the trajectory location. (Arrow is simply a symbol, not a description of uncertainty.) The remaining sequence of maps (Figures 2b, 2c, 2d, and 2e) show the development and propagation of the southern global plume, which was eventually sampled in the positions discussed in Figures 1 and 3. Double-headed arrow marks position of kinetic trajectory reaching back to South America in Figure 3. A small white asterisk near northern New Zealand in map in Figure 1a marks the origin of a ''clean'' parcel described in the text. The clean trajectory was described in Figure 3. (a) Modeled situation at the time of sampling, 24 September. (b) 12 September, 0000 UT, 7.5 km. (c) 14 September, 0000 UT, 7.5 km. (d) 16 September, 0000 UT, 7.5 km. (e) 18 September, 0000 UT, 7.5 km. (f) 20 September, 0000 UT, 4 km. Flights are labeled by starting date.

compensation level of somewhere below 40 ppb, and even more is produced within a biomass-burning plume with increased levels of methane and other organics. The behavior of our CO tracer in this simulation is therefore of an accumulating tracer whose concentrations are kept bounded by the 50-ppb northern and southern boundary conditions; the boundary conditions and the length of simulation tend to set a reasonable level of nonplume CO. These boundary conditions were suggested as the simplest possible background consistent with the TRACE-A, PEM-Tropics A, and MAPS ''background'' data [*Chatfield et al.*, 1998; *Pougatchev et al.*, 1999]. Details of the lowest values therefore differ slightly from the TRACE-A simulation, which had the benefit of aircraft profiles of observed CO near the boundaries of the simulation. The background concentrations were applied at the north and south latitudes shown in Figures 1 and 2, i.e., $\sim$30°N and 50°S for PEM-Tropics A. Uncertainties in the plume nitrogen and oxidation chemistry of the PEM-Tropics A series [*Schultz et al.*, 1999] also limit what we might gain from using complete chemistry. Detailed investigations are beyond this work; here we are trying to use an available model to focus on process and mechanism.

[18] One example is also presented from the PEM-Tropics B flight series (March 1999), and in this situation, CO was treated as a reactive tracer. Several aspects of this simulation, including characteristically longer transport times, made the reactive tracer appropriate. Details of CO's parameterized sink (and of its described source from CH_4) and the incorporation of more detailed boundary conditions are presented by R. Chatfield et al. (manuscript in preparation, 2001).

3. Technique Development, Results, and Discussion

3.1. Midtropospheric Plume Studied With a Combined Technique

[19] Let us focus on one particularly interesting interception of a continental plume and use it to illustrate the coordination of tracer and trajectory analysis. This will illustrate the strengths and present limitations of a simulation and analysis technique we propose for use in understanding long-distance transport.

[20] Let us examine the case. During flight 14 the DC-8 made a north-south survey along the 179°E meridian. Such meridional transects proved to be valuable flights in PEM-Tropics A since they sketched out broad meridional meanders of pollution that were approximately cross plume. Figure 3 illustrates a vertical profile ob-served as the aircraft gained altitude slowly. Values of computed CO interpolated to the aircraft position are also shown.

[21] Figure 3 additionally shows a selected vertical profile from a single column of model points selected from the grid near the position of the slow descent. The model grid levels are visible as the crosses marking this line. This column, $\sim$200 km to the east, tends to better match the shape of the lower part of the profile, 1–3 km. Note that these model column plots do not suffer from the smoothing inherent in interpolation to the flight path. The interpolated values near 7 km and the profiles near 4 km are similar to the observed profile in shape, although the magnitude of variation is reduced.
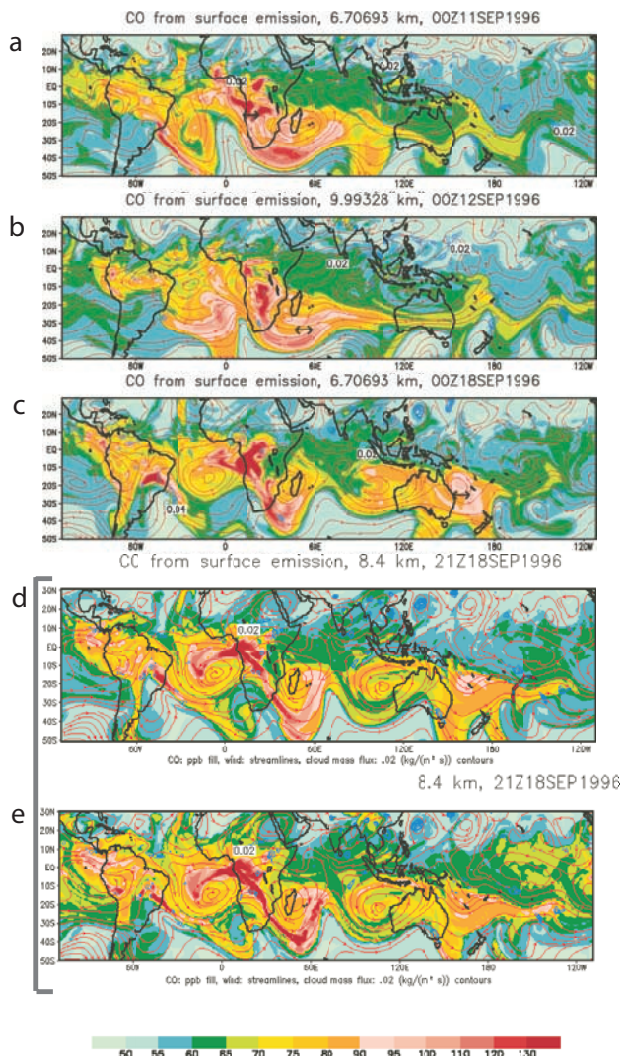
Figure 2. Simulated spread of the "megaplume" event from Africa to the eastern Pacific on 18 September. Final position is shown in (d) and (e), which reflect different simulations (see section 3.3.2). (a)−(c) Significant points in the transit of the megaplume from the southern Africa region, with approximate trajectory points marked by the double-headed arrow (orientation is not significant). Figure 2a shows pollutant venting over central Africa in a complex meteorological pattern. By 12 September (Figure 2b) the parcel is closely associated with a warm frontal feature mentioned earlier trailing downwind from the south coast of Africa. Figure 2c shows the next significant complication of the meteorological evolution as the selected trajectory passes by a small closed circulation center northeast of Australia. Small errors in simulation at this point would make considerable differences in final distributions. This is partially shown in the final panels only 21 hours later. Figure 2d shows the sampling track of the aircraft (red indicates that the aircraft is below the map level by >1 km, and blue indicates that the aircraft is above). Several differences between the different simulations shown in Figures 2d and 2e are described in section 3.3.2.

[22] Perhaps this ability to match different parts of the profile with different simulated columns is indeed attributable to skill in modeling. It is reasonable that the simulations are suffering from only slight errors in wind shear accumulating over tens of thousands of kilometers. (How slight? An average error in mean wind speed of only ∼0.3 m s^{-1} over 1 week's trajectory would allow for the 200-km offset. 1 m s^{-1} would appear reasonable.) Alternatively, the reason might be simply that we can select a good match and quit when one is found. (We call this a "fishing" hypothesis and will consider it below.)

[23] It is beyond the scope of this paper to construct and execute a statistical test to demonstrate skill in matching profiles, i.e., the coincidence of high and low points in the vertical. Simple histogram analysis of observed and simulated distributions is presented at the end of the paper and suggests that simple statistical properties agree fairly well.

[24] Additional information can be found in tracer maps. The tracer model also provides information about the shape, context, and origin of these plumes. Figure 1a (at the top though temporally the end of the Figure 1 sequence) shows a map view of the lower tropospheric plume, 3.3 km altitude, obtained from our GRACES run. A wispy trace of the plume can be seen crossing the 179° line, especially just to the east of the line. Mapped concentrations reach 70−75 ppb just to the north of the aircraft position, though the interpolated values shown in Figure 3 are far short of the observed 80 ppb. The elongated nature of the contours suggests that this same general plume may have been sampled by the DC-8 more than once, and we will present some evidence for this.

[25] The other maps, Figures 1b, 1c, 1d, 1e, and 1f, suggest a plausible origin for the pollutant plume sampled by the DC-8; the mechanism is discussed below. If correct, their wealth of visual detail summarizes considerable information about source mechanisms and the weather patterns of transport. First, however, we must describe how we backtrack in space and time to select these maps.

[26] Now let us consider the uncertainty that seems to arise when we consider swarms of trajectories. The origins of the plume at 3−4 km can be traced back in several ways. We could possibly attempt to trace a maximum feature back through the maps. This procedure turns out to be difficult: It is hard to trace maxima in three dimensions, and dispersive and confluent aspects of fluid motion can lead to errors. Back trajectories are a familiar and useful technique for this source tracing. Henry Fuelberg and his Florida State University associates [*Fuelberg et al.*, 1999; *Board et al.*, 1999] have constructed trajectories based on ECMWF analyses recorded every 12 hours; wind changes that may alter the trajectory significantly may only be assessed by interpolation in time.

[27] The work of *Board et al.* [1999] and discussions in a TRACE-A special issue [e.g., *Pickering et al.*, 1996b] illustrated two known facts: (1) backward trajectories from points quite near in horizontal and vertical scales may go back to widely different source regions, and (2) the effects of differing meteorological analyses and different trajectory construction techniques (e.g., isentropic; "three-dimensional") will give different source regions in certain cases. When a large swarm of back trajectories is drawn from a large grid surrounding, e.g., 500 km from the observation
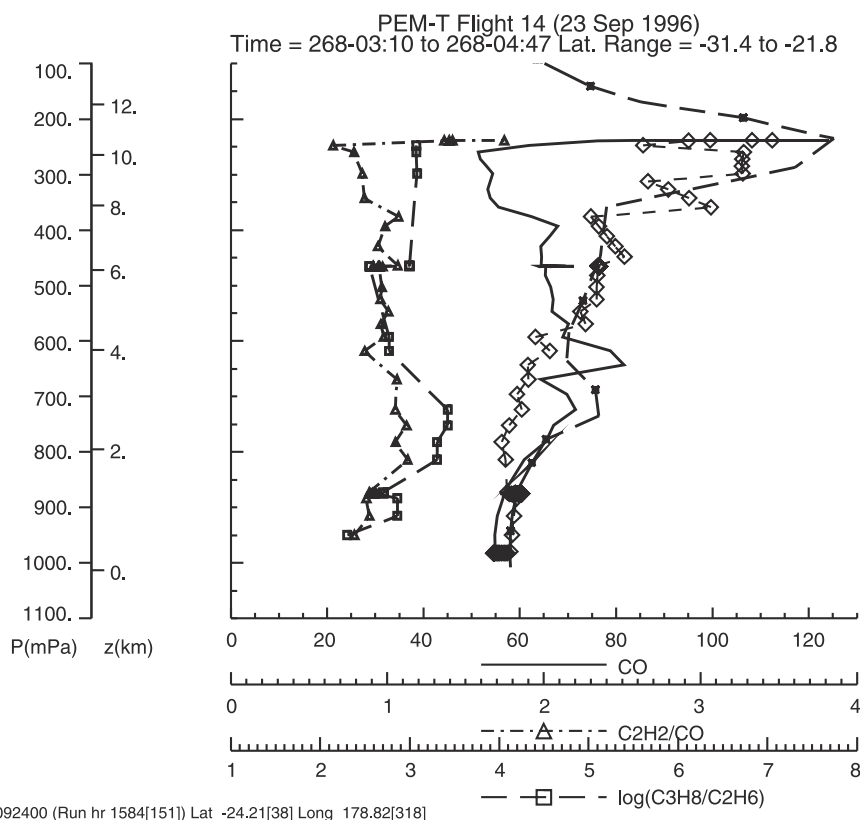
Figure 3.   Vertical profile of carbon monoxide observed on board the DC-8 on 24 September 1998, for the flight labeled by starting date, flight 14, 23 September, near the International Date Line (179°W, 34.5°S to −32.1°S latitude, 0200–0300 UT) by G. Sachse/NASA Langley differential absorption CO measurement (DACOM) instrument. Also shown are profiles interpolated from the model history files along the aircraft flight path (diamonds), and also from nearby model grid points, at 25.9°S latitude, 178.8°W longitude (crosses at model grid levels and dashed lines). Note that these plumes have generally similar shapes but greatly reduced variability compared with the observations. Another nearby model column exhibits the profile measured in the lower troposphere.

point, the origins of concentration features seems very uncertain, as some of the origins are widely divergent. This suggests a rather broad uncertainty in plume origins that has influenced analyses of NASA's DC-8 and P-3 and similar aircraft data. We will argue that uncertainty is much less most of the time and is especially so in remote areas like those sampled by the PEM-Tropics expeditions.

[28]   A guided trajectory analysis is proposed to ameliorate uncertainties in many situations. The three trajectories of Figure 4 are specifically selected trajectories, and this is a departure from a common practice these days of showing swarms of trajectories. First, we present some specifics of our calculation. Trajectories used the hourly wind and cloud occurrence history reconstructed by MM5; in these the weather simulated closely approximates the ECMWF analyses by the data-nudging process, but the winds used are consistent dynamical winds provided by the mesoscale model every hour. Several such trajectories are shown in Figure 4. The MM5 trajectory package we used has a basic control option that allows it to degrade to approximate isentropic trajectories; however, we included the nonisentropic effects estimated by MM5, principally, radiative cooling and occasional warming associated with frontal cloud motions. Evaluation of equivalent potential temper-

ature along the trajectory helped us to evaluate its consistency with the underlying model.

[29]   The use of the MM5 and GRACES together allows us to work easily with another source attribution technique that seems to allow us to select consistently more plausible trajectories. To do this, we make use of the simulated CO-tracer fields shown in the maps. For any CO peak observed by the aircraft we initiate back trajectories from those few points in the simulated tracer field, not necessarily exactly coincident with the sampling point. They start from points that (1) do contain high-simulated concentrations of CO and (2) are as close as possible to the true aircraft sampling point. The trajectories then are traced back. Three trajectories starting from a high-pollutant point near the sampling point are shown in Figure 4; each one leads back to Africa, and one leads to South America. One trajectory was started from the point in a low-concentration marked by a small white star in Figure 1a; trajectories, not surprisingly, lead back to a clean area in the Southern Ocean near New Zealand. Often both trajectory and tracer techniques tend to give a consistent history of the plume for a long distance: both trace the plume to southern Africa and, beyond that, the polluted South Atlantic region. In some cases that follow, we shall glimpse some examples showing how far
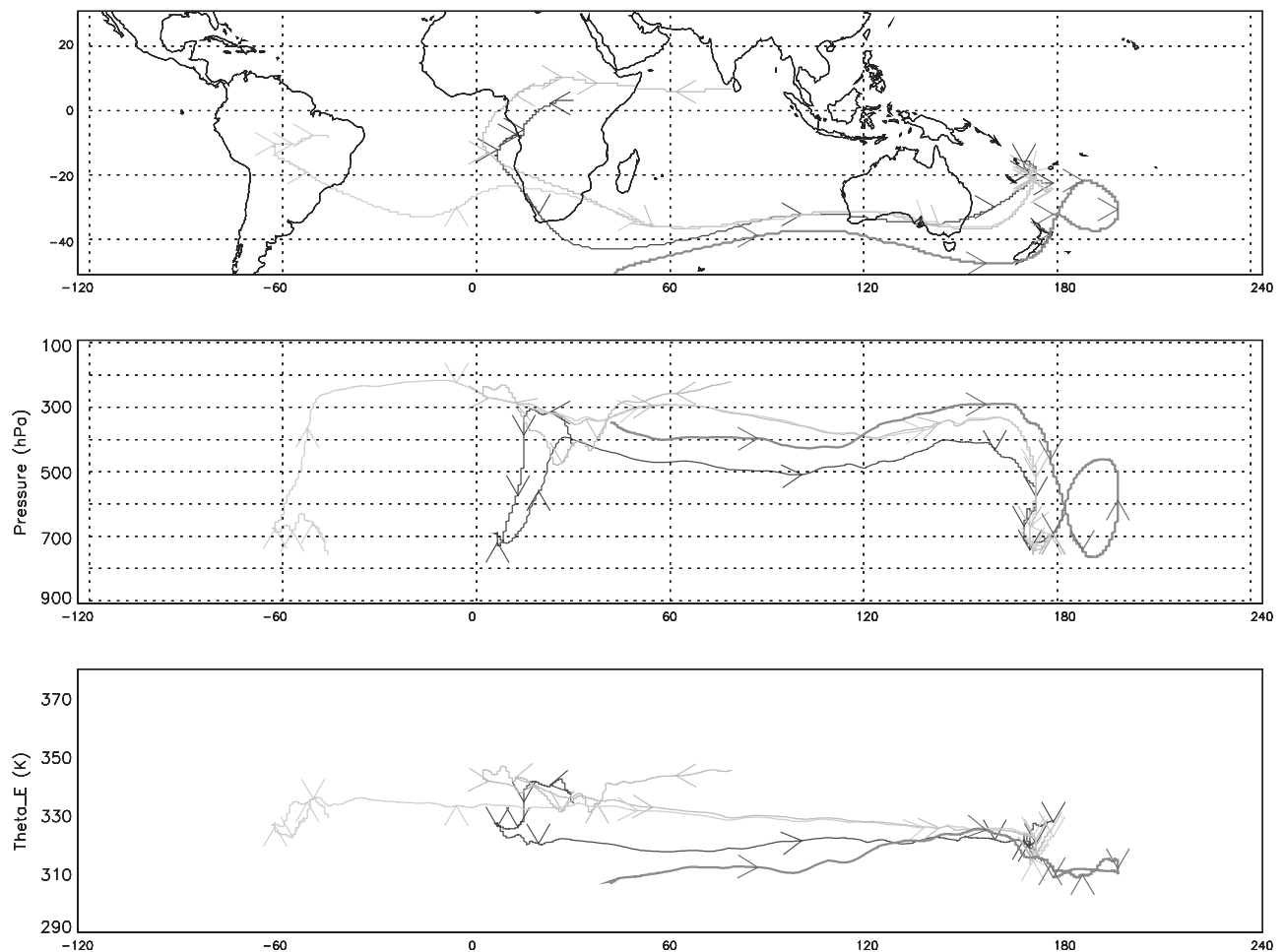
Figure 4. Back trajectories from several points along and near the region of DC-8 descent of 23–24 September 1996 and a comparison clean point slightly to the east in the Pacific Ocean. (a) Map showing trajectory coordinates. Note that bottom trajectory, drawn from a clean region, also has a clean origin out of the Southern Ocean. (b) Altitude of parcels in pressure units (hPa). Arrows are plotted showing instantaneous direction every 2 days backward from the final sampling point, e.g., at 6 September, 4 September, 2 September, etc. Direction of arrow marker is not significant. In Figures 3a and 3b, regions of trajectory looping and hesitation are those most typical of a larger selection of trajectories not shown: South America, over central Africa, and then again in the Pacific east of New Zealand. Looping does occur in other regions but more rarely. (c) Pattern of change of θ_e, equivalent potential temperature, in K. Near conservation in this variable suggests that the trajectory is believable, not crossing into other air masses. Slow decrease in θ_e is due to radiative cooling simulated in the MM5 model using the Community Climate Model 2 (CCM2) radiation scheme. The region of complex motion over southern Africa also shows greater variation in θ_e.

back these differences become significant; in the cases we chose to study, often just west of Africa, it is >15,000 km away! Figure 1e shows that the above guidelines (1) and (2) do not provide a unique choice for back trajectories (possible end points along the simulated pollutant plume are extended along a curve near the sampling point), but they do spotlight strong choices; strict use of guideline (2) would specify the closest point along the curve. Furthermore, the patterns within the maps tend to remove some mystery surrounding the tendency of trajectories to diverge. For example, the maps show that fast-moving pollution streaming in a jet from South America can be joined by pollution arising from Africa (Figure 2c): Such subtropical jet streaks often seem to filament together.

[30] Our trajectories of plume features do wander somewhat from local maxima in the tracer map even though they are based on the same reconstructed winds. The reasons seem to correspond with the different numerical grids and interpolation assumptions that are needed to make each reconstruction. Numerical techniques for tracer transport are also a compromise between accuracy considerations appropriate to trajectories and other requirements, e.g., minimizing spurious numerical diffusion.

[31] Using tracer maps and trajectories together tends to focus our attention on specific source regions. The possibilities of other source regions affecting the sampled area are shown graphically in the tracer maps. This partially addresses the critique that we are just "fishing" (see

discussion of Figure 3). Note that the concentration maps (including those for atmospheric layers not shown) suggest that the number of distinct possibilities (high-concentration regions) among which to fish is limited, and that the origins of these high-concentration regions are very similar. In brief, there are very few fish in this sea, and they are concentrated into only one or two "schools." There remains the possibility that the reconstruction of weather is rather far wrong. For example, the effects of a compact circulation system might be totally missed in the weather record used to constrain MM5, despite the use of global satellite data, and that therefore a complete class of trajectories (as well as a complete stream of high tracer concentrations) is missing from the reconstruction.

[32] Of course, tracer analyses attempt much more information than trajectories. The tracer technique also explicitly quantifies concentrations for air parcels that come from the complex sequence of biomass burning (or other pollution) followed by deep convection and long-distance nearly non-dispersive transport.

3.2. Plume Transport Processes: 24 September 1996

[33] Now let us follow the tracer simulation forward in time using the MM5 reconstruction trajectory information to find an approximate plume starting point. Our analysis of tracer maps derived from high-resolution MM5 studies suggests that similar histories explain many of the plume encounters enumerated and described by *Staudt et al.* [2001] and others. Figures 1b, 1c, 1d, and 1e show a set of maps of simulated tracer CO for positions selected to follow the trajectory extending back to South America in Figure 4a; we will discuss this choice in the following paragraphs. Maps at the model's level nearest to the trajectory position are shown. These trace the history of material from the South Atlantic–southern Africa source region to the observational point near the international dateline. The earliest-time panel, Figure 1b, shows the situation of 10 September, 14 days before the DC-8 intercepted the plume near the 180° line.

[34] The situation shown in Figure 1b is observed in our 2.5-month reconstruction. The blue contours marking cloud mass flux over southeastern Brazil, directly under the trajectory marker point, show a trailing region of enhanced CO. The venting has been occurring for some time, so that a large area along a northwest-southeast arc has built up to ~130 ppb. The form of the arc suggests that the convective venting locations and blow-off were strongly controlled by the subtropical extension of a cold front. Here, synoptic (model grid resolved) and cloud-scale (subgrid) processes actively cooperated with each other in this lifting; the narrowness of the simulated feature suggests that cloud-scale lifting may have predominated. *Chatfield and Delany* [1990] suggested subtropical frontally organized convection as one of two most likely fates for the biomass-burning pollution that accumulates over South America. Frontal activity is common. Another linear feature off the southern coast of Africa in Figures 1b and 1c suggest warm frontal activity. We will return to this feature later.

[35] Another fate highlighted by *Chatfield and Delany* [1990] involving central tropical convection is illustrated in Figure 2. Many descriptions of this cumulonimbus mecha-

nism have been published. The cases illustrated by *Pickering et al.* [1996a] and *Jenkins et al.* [1997] and put into context by *Scala et al.* [1990] were more like this deep-tropical cumulonimbus venting without frontal organization. (Of course, as the dry season breaks down in September, the distinction between tropical and subtropical becomes less defined.)

[36] The accumulation and venting process is episodic but repeated. Similar accumulation of CO at 3.3 km in Africa and South America is shown in Figure 1a (when our plume has reached its Pacific sampling point) and indeed, another subtropical venting process seems to be developing. *Chatfield et al.* [1996] described the process of accumulation and venting in Africa. That paper and other observational papers by *Jenkins et al.* [1997] remarked on the deep extent of mixing, above 3.3–4 or even 5 km associated with biomass-burning pollutants over the drier African lands. The lower concentrations shown over much of the Brazilian Cerrado in Figure 2a occur because fair weather mixing does not penetrate to the level shown.

[37] Now the narrative turns to situations with confluent trajectories and with some evidence of that they are concentrated in certain regions. Following our air mass from Figures 1b and 1c 3 days later, 13 September, the CO-rich air mass has crossed the Atlantic and is visible at 8.4 km over the Namib coast. This map was chosen to illustrate the confluence, or stranding together, of two plumes, seen reaching 90 ppb. Off the coast to the west of the trajectory mark the somewhat separate origins are particularly clear. Indeed, two trajectories in Figure 4 with very close endpoints diverge, one looping back over Africa. Hints of its origin may be seen in the previous frame (Figure 1b) in a pollutant accumulation near the equatorial coast of the Congo region. The slowness of the plume's progress and the complexity of the motion make us hesitate to follow the plume. The trajectory shown indicates that pollution influence from South Asia is even possible in this case. Our experience in modeling both the TRACE-A and PEM-Tropics A suggests that generally, the pollution buildup has an African origin. Modeling papers for TRACE-A by *Jenkins et al.* [1997] and *Chatfield et al.* [1998] have described these accumulation patterns: In Africa the continental accumulation brings accumulating pollutants from southern, eastern equatorial, and eastern central Africa into a convergence-divergence region, often near the western equatorial coast.

[38] To summarize the process so far, previous work and this analysis suggest (1) continental accumulation and (2) characteristic convergence-divergence patterns (frontal convection, the Inter-African Convergence Zone (IACZ) [*Chatfield et al.*, 1996] are points (1) and (2) of our suggested general pattern. This work illustrates our observations, which are based on the entire 2-month simulation of these general patterns: (3) a tendency toward intercontinental accumulation in the South Atlantic and (4) occasionally, a final injection of highly polluted material as air crossed southern Africa (see again Figure 1a), with output between 9 and 15 km.

[39] The narrative now turns to the particular meteorology of the Indian Ocean and rapid, seemingly "ducted" transport. The pace of trajectory motion continues rapidly out to the central Indian Ocean with our trajectory marker moving to ~100°E by 15 September. Figure 1c shows a

large plume migrating rapidly and directly across the Indian Ocean in a westerly jet. In this equinoctal season, there is no strong drift due to monsoon forcing from Asia or Australia and the small likelihood of encountering the complicating effects of equatorial storms. Figure 1d, two days later on 17 September, shows a distinct plume maximum that has just crossed west central Australia to a point just northeast of New Zealand.

[40] The rapid, direct motion up to this point illustrates our general observations listed in the introduction: (5) rapid and undilute, undulating transport and (6) subsidence of the plumes. An expected slow radiational subsidence in equivalent potential temperature (θ_e) is notable in the upper two African trajectories starting about 10 September. The effect on the pressure altitude is modulated by waves in the subtropical jet.

[41] In this map, on 17 September the parcel is still speeding along high in the midtroposphere near 8 km. Suddenly, the eastward motion slows dramatically as the trajectory moves past 160°E. Figure 1f (19 September) shows the trajectory parcel as it begins to be caught up in a local trough, moving down to the vicinity of the 4.6-km region which is mapped. While the eastward propagation slows, equatorward motion is accompanied by characteristic downward motion. Meteorologically, the features of this motion are consistent with near-adiabatic motions under the conservation of potential vorticity. The equivalent potential temperature for the parcels (Figure 4) changes slowly (due to radiation). This gives us some confidence that motions are tracked consistently by the tracer models and the trajectory analysis despite the complexity of the motion.

[42] There is very little net motion leading to the final sampled position on 24 September. The maps suggest that the simulated plume becomes largely attenuated and broadened in these final 4 days of complex motion, dispersing into a wispy structure evident in Figure 2a. On the maps the highest concentrations associated with the parcel drop from >90 to 75 ppb or less. Apparently, the observed plume did not disperse nearly as much, reaching to nearly 120 ppb. Despite the attenuation the motion of the pollutant maximum plumes illustrates the general features (6) and (7) of subsidence and increasing undulation and dispersion within the Pacific Ocean atmosphere. In this case, nearly 150° longitude was traversed by the South American parcel in 7 days (Figure 2e), and only ~20° in the final 7 days.

[43] As we have seen, this study of progress of the pollutant plume from the South Atlantic/southern Africa pollution source to the observation point illustrates many common features of such southern plumes. There are many variations on the plume behavior that we cannot detail, but our generalizations (1–7) seem to characterize many of them.

3.3. Tracking the Megaplume as Sampled on 18 September
3.3.1. Similarities in Transport Pattern

[44] The DC-8 sampled a particularly strong segment of the southern global plume on 18 September. Concentrations reached 120 ppb and reached 160 ppb in one restricted region, at 23° and 27°S at 165°W, i.e., northeast of New Zealand. *Staudt et al.* [2001] note a general connection between this plume and several others sampled during

PEM-Tropics A, including the 24 September plume, which was just described. The sampling situation is shown as the final frame of Figure 2. There is a maximum concentration shown in the area, but the magnitude is only ~85 ppb. Clearly, the simulation was unable to capture the magnitude of the plume. Still, the analysis of weather and simulated concentrations suggests both the origin and a reason why the meteorology might have been particularly difficult to trace exactly in this region. The top two frames show one back trajectory from a plume maximum in the area. The greater than symbols indicate 2-day intervals; of course, the timing of this trajectory must be considered an approximation to the true timing of transit. The first panel suggests a pollution source in west central Africa: the tropical, deep convective pattern of lofting. This occurred on 11 September. One day later, at 00:00 UT on 12 September, the trajectory suggests strong additional influences by a feature that appears to be very strong (120 ppb) and the wide area of influence suggests frontal activity below. We have mentioned a similar feature in Figure 1 and will describe the pollution-spread pattern more below. In the ''ducting'' pattern we have previously described, the sample pollution trajectory has reached the eastern coast of Australia by 18 September, only 6 days later.

[45] Only at this point does the wind field become more complex. The streamlines suggest that a small anticyclone has formed, and the pollution pattern becomes broadened. Any uncertainty in the reconstruction of the wind field in this tropical ocean region would be reflected in redirection of the simulated plume from its true path and possible undesired breakup of the concentration maximum field. The displayed concentration maximum has already decreased from >110 ppb off the coast of Africa to >95 ppb.

[46] Our study of several situations like this suggests that it is the passage through these regions that makes simulations, whether trajectories or tracer maps, less certain. These encounters, not the length of the trajectory, should be the norm for judging the degree to which trajectory attributions may be considered somewhat reliable. The common practice of accepting back trajectories up to only *n* days (*n* = 2, 5, 10. . .) would be this view, just an averaged statement of the likelihood of encountering more of these regions of complex flow. (The reconstruction of 6 days from 12 to 18 September would be more convincing than the last day's journey from 0000 to 2100 UT and the final sampling.) The reader may gather from the streamline patterns seen in our map panels a more general truth that we see in the whole sequence: Patterns of complexity, dispersion, and trajectory splintering tend to occur over Africa, especially the western south coast and east of northeast Australia, approaching the base of the SPCZ.

3.3.2. Sidelight Case Study: Nonburning CO and Variations in Transport Simulation

[47] The last panel of Figure 2 provides a minor case study describing appropriate questions: What are the effects of interpreting the wind data slightly differently, e.g., using different numerical transport techniques? What is the consequence of omitting urban industrial pollution sources? Otherwise, the panel shows the same situation as the panel above it.

[48] The bottom panel includes these sources; it also shows variations that result from an alternative numerical transport scheme [*Walcek*, 1999]. The Walcek scheme
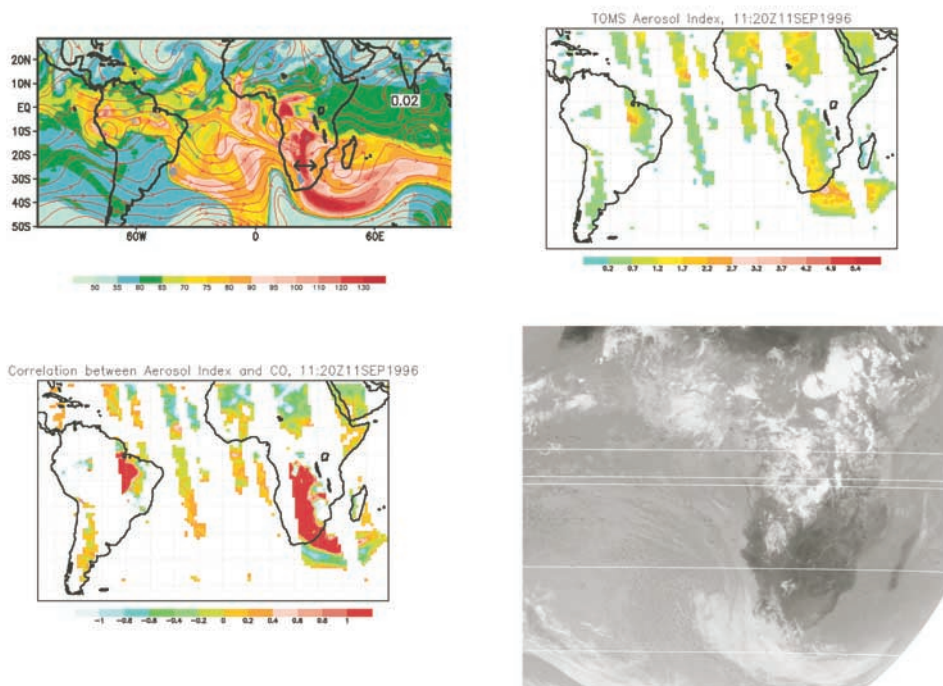
Figure 5. Simulated origins of the megaplume event that was later sampled by the DC-8 aircraft on 18 September along with observational data supporting our attributions. Upper left, simulated CO field in the midtroposphere at 1200 UT on 11 September 1996 with an approximate marking for a back trajectory for a parcel eventually sampled (see Figure 4 and section 3.3.3). Upper right, Total Ozone Mapping Spectrometer (TOMS) estimate for aerosol index (AI) [*Torres et al.*, 1998] for approximately the same time; in the southern region this index responds to smoke-absorbing aerosol, while in northern Africa the index probably indicates absorption due mostly to dust. Note the great coincidence of these patterns of biomass pollution. Lower left, contributions to the correlation of the calculated CO and estimated aerosol index (terms summing to the spatial correlation coefficient of the mapped samples CO_i and AI_i: $(CO_i - \hat{m}_{CO})(AI_i - \hat{m}_{AI})/\hat{s}_{CO}\,\hat{s}_{AI}$. Note the high values of these contributions (red). The tendency toward anticorrelation (green, just below the red) is also noticeable. Lower right, Meteosat visible infrared image of this region indicates the large cloud shield accompanying the warm front is obscuring much of the aerosol index from remote sensing, explaining the green negative correlation regions.

characteristically produces slightly faster plume movement, and some features are more clearly delineated. To the extent that we can compare the two schemes using the observed CO data, the Walcek scheme seems to be slightly more accurate in its phase speed. For the period of 18–24 September, slightly lower altitude plume transport is also simulated, improving certain data comparisons where we may have difficulty (Figure 3).

[49] Also, this example suggests that there is somewhat greater effect of central and northern South America emissions than our main simulation technique indicates. The area >65 ppb, colored green-yellow near 120°W around the equator, is noticeably larger than with our standard, the Smolarkiewicz transport scheme [*Smolarkiewicz and Grabowski*, 1990].

[50] The differences noted suggest that rather subtle differences in the use of the wind data can have moderate affects on the features of simulations out to 4000 km (e.g., the large region >65 ppb). However, the distributions of the panel show that the urban industrial sources within the region do not affect our picture of the southern global plume greatly, and so we have not redrawn all the maps.

3.3.3. Synoptic-lifting Origins of The Megaplume of 18 and 24 September

[51] The maps suggest that the specific plume origins we have described so far are quite typical; plumes continue to emanate from South America and Africa throughout all the maps with occasional interruption. However, the observed magnitude of the peak concentrations of these plumes makes their origin especially interesting, and the plume has also been discussed by *Staudt et al.* [2001]. Let us consider the source of the large episode in more detail.

[52] Figure 5 shows the analysis of our tracer model for CO for 12 September at ~1200 UT. Figure 5 also provides other evidence that the model is capturing some of the fine details of the pollutant lofting and transport process. Figure 5b provides an analysis of the TOMS aerosol index for the region, and Figure 5d shows the Meteosat infrared image for the period. The TOMS aerosol index is an indicator of the ultraviolet light absorption by aerosols [*Torres et al.*, 1998] with best sensitivity in the middle and upper troposphere. Black carbon and other compounds in smoke are the most likely explanation for the absorption in this region, though in
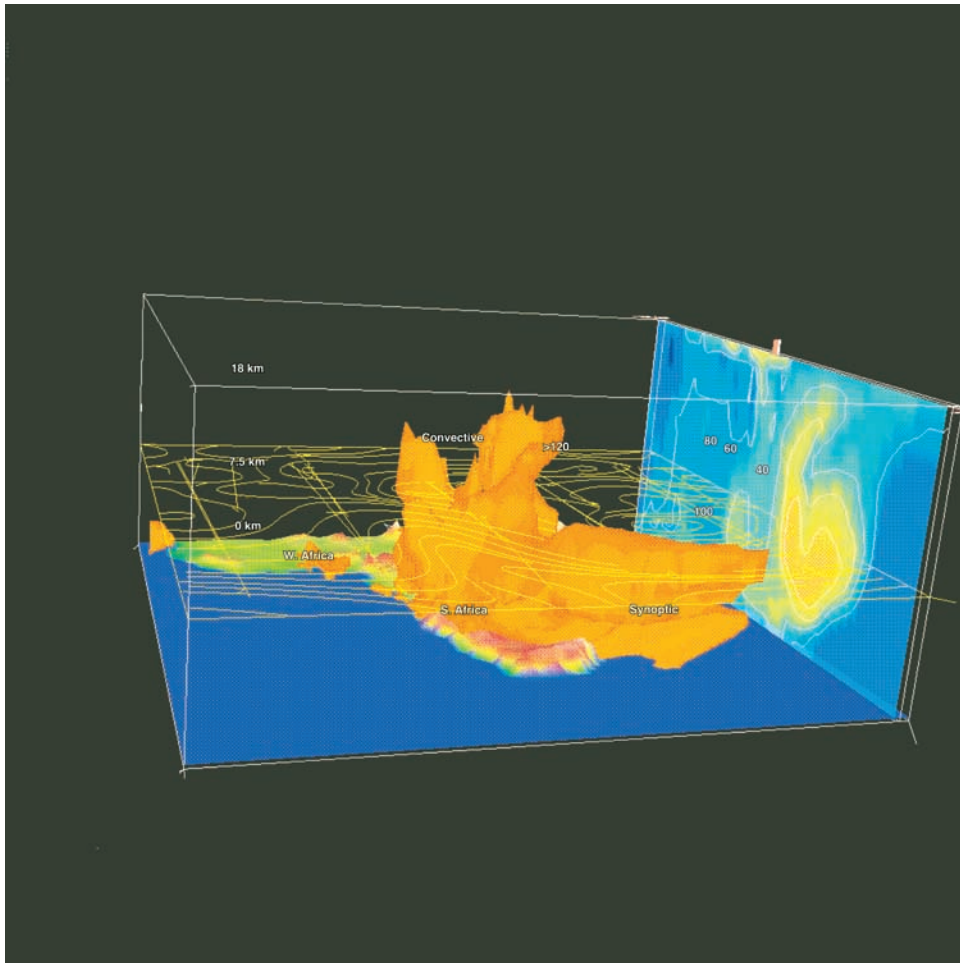
Figure 6. Global Regional Atmospheric Chemistry Event Simulator (GRACES) reconstruction of the 3-D lofting and spread of a very concentrated plume from central and southern Africa, as portrayed with Vis5D software. The orange-colored volume describes the region with over 123 ppb of simulated CO, obscuring most of southern Africa. Contours in the right panel describe the southern global plume exiting to the east, with indicated concentrations in parts per billion. Tropical convective lofting, extending to the uppermost troposphere, was simulated by the interpretation of subgrid-scale cloud vertical mass fluxes. Subtropical synoptic lofting was resolved by large-scale winds. The wind pattern at 7.5 km is also indicated by streamlines (note the algorithm produced some extraneous lines); visualization by Vis5D.

other regions, e.g., west Africa north of the Sahel, dust is more important. Both smoke and CO are emitted by fires, and their concentrations are correlated, especially where cloud processing has not rained out the aerosol. The outlines of the regions affected by high simulated CO and the observed aerosol index are remarkably similar. Figure 5d indicates a large mass of storm clouds in the Southern Ocean to the south of the maximum in aerosol index. In this region, smoke could be either scavenged or hidden by cloud, and consequently, we would not expect good correlation. These contributions to correlation and anticorrelation are shown in Figure 5c.

[53] Cyclonic storms, not individual cumulonimbus, are implicated in this case. The extended cloud band in the geostationary satellite image shown in Figure 5 emphasizes the type of synoptic-scale uplift that appears to be especially effective in bringing about the pollution of the upper troposphere. A more comprehensive view of this can be seen in the 3-D view shown in Figure 6. In this view the

discrete, very high lofting patterns shown for central Africa are distinguished from the extensive patterns found southward in the region of the synoptic extratropical-type warm front.

[54] *Staudt et al.* [2001] point out the anomalous high concentrations of CO and other species associated with this plume as sampled in the West Pacific and indicate how different are the concentrations of CO associated with the cloud-scale and synoptic-scale lofting mechanisms. At times, CO concentrations of 120 ppb were found even this far downwind. The cloud band of Figure 6 indicates a large region of synoptic uplift along an east-west warm front.

[55] Figure 7 shows several stages of the transport pattern. Panels on the left show the surface pressure and wind field patterns on 11 and 12 September in the early afternoon, while the right panels show the effects at 2.7 km altitude, portraying both simulated CO and wind streamlines. On 11 September the long-distance accumu-
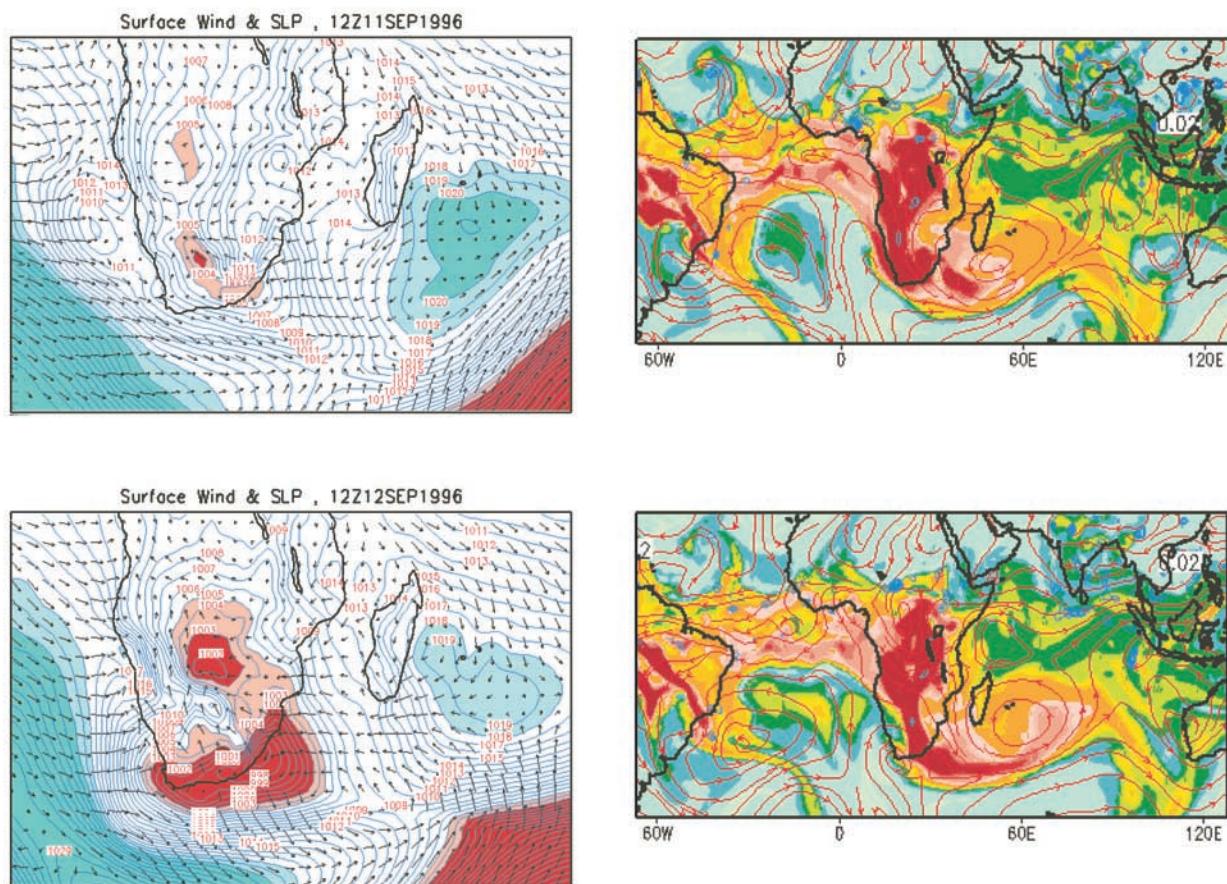
Figure 7. Meteorology of the origins of the megaplume sampled by the DC-8 in the western Pacific in a very large region of accumulation over equatorial and southern Africa. The left panels describe MM5 reconstructions of sea-level pressure and surface wind vectors, while the right panels describe GRACES portrayals of carbon monoxide and wind streamlines at 2.7 km. Note both the extensive region of accumulation of pollution and the large-scale pattern of pollution lofting in South Africa and just offshore. Vertical wind analyses (not shown) correlate with the pressure contours shown in a classic warm frontal pattern.

lation of CO moving southward over much of central and West Africa is apparent; earlier, there was flow from eastern Africa and Madagascar. Anomalously large fires anywhere along this large collection region could account for the >120-ppb CO concentrations flowing out and eventually measured out in the western Pacific. On 12 September the lofting in the large low-pressure system is visible.

3.4. Evidence for Subtropical Plumes in Spring

[56] What happens to the southern global plume in other seasons? During the summer and winter the powerful monsoon circulations dominate the Indian Ocean region. The east-west flow of the southern global plume may be interrupted by a predominant north-south flow (simulations shown in the model of *Bey et al.* [2001]). In the austral autumn, however, there is again an opportunity for a subtropical duct similar to those we have seen. In fact, the Global Tropospheric Experiment (GTE) aircraft returned to study the Pacific in this period in PEM-Tropics B, March– April 1999. In one instance the DC-8 aircraft did apparently sample a plume originating many thousands of kilometers to the east, out of Africa. Figure 8 shows the path of the DC-8 on 22 March 1999, as it sampled this long-distance flow in the western Pacific. Our map of the 8-km region shows a broad region of somewhat enhanced CO to 50 ppb. Our trajectory analysis from this region traces this air back to near Africa over a period of 10–12 days (see Figure 9). The winds of this period are apparently much slower; our 3-D trajectories suggest slow sinking motion until the last day or so, when movement toward the equator raises the trajectory slightly. Figure 9 suggests an origin near Madagascar around 28 February to 2 March, and our simulations suggest that convection was rather frequent in the region at that time, though we have not suggested one specific source.

[57] This sample of the southern global plume from the continents was low concentration (only ∼50 ppb), diffuse, and only sampled in the westernmost area of the Pacific. True, the source for CO in the southern continents is low
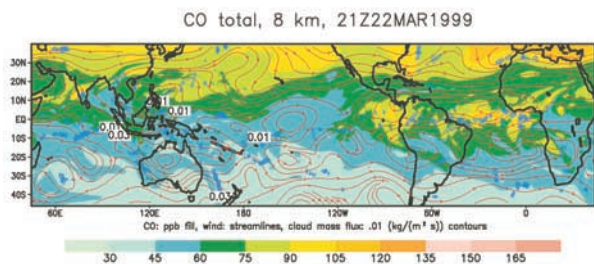
Figure 8. Transport patterns associated with the lofting of the megaplume concentrations. Map of simulated CO at 8 km from PEM-Tropics B, 22 March 1999. This map is an example of the subtropical continental plume in the austral autumn (i.e., boreal spring). Note the penetration of the weak subtropical plume (blue colors to 60 ppb) to the westernmost South Pacific. Trajectories indicate this origin. As the wind streamlines indicate, the flow is already beginning to curve and distort.

during this time, not the burning season; perhaps other continental tracers would show more of a plume. The whole pattern of the simulations for the period suggests that this limited propagation of the subtropical plume is a general characteristic for austral autumn. Indeed, the higher concentrations of CO in the region the DC-8 sampled seem to have differing sources. The simulation suggests these ori-

gins: (1) in the boundary layer, flow in from the Northern Hemisphere, as suggested by PEM-Tropics B analyses (R. Chatfield et al., manuscript in preparation, 2001); (2) at intermediate levels, flow from the west, as our trajectories suggest; (3) at upper altitudes, influence from tropical convection over Indonesia, north Australia, and adjacent islands.
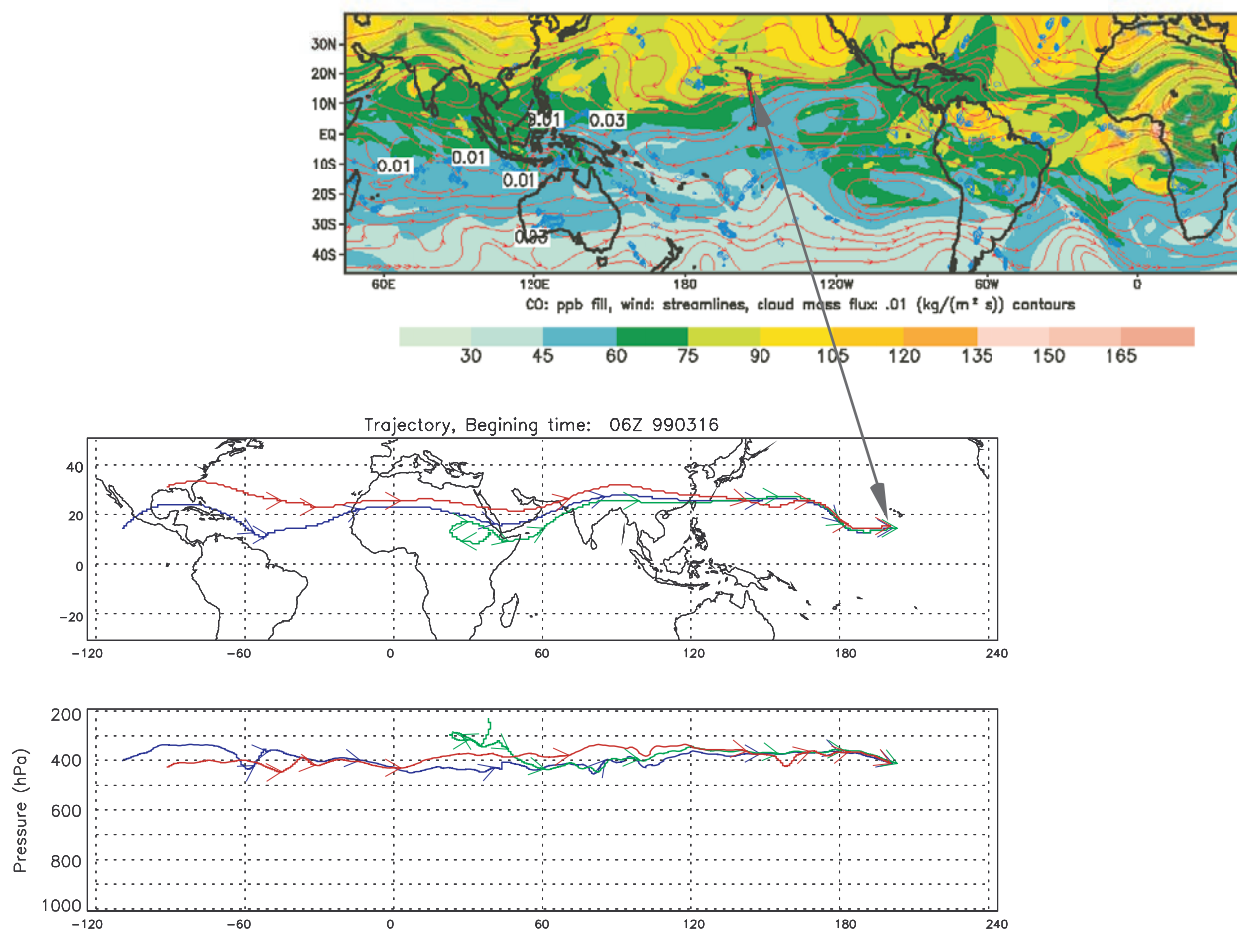
3.5. Extended Subtropical Plumes in the Northern Hemisphere

[58] Figure 8 portrays not only austral autumn but also, of course, boreal spring. If the spring period, with its predominance of biomass burning, is the great period for extended plumes, can these be seen in boreal spring? Figure 8 suggests that such plumes do exist and derive from India as well as northern Africa and perhaps nothernmost South America. Figure 10 shows a possible encounter with a northern global plume originating out of Africa or South America. CO was measured to be at $70-80$ ppb as the DC-8 flew through the area at $8-10$ km. The plume was relatively old, if we believe the evidence of tracers that indicate time since emission. This age is based on their differing reaction with OH ($C_2H_2/CO \approx 0.5 \times 10^{-3}$ and $-\log(C_3H_8/C_2H_6) \approx 3$). Regions to the north appeared to be more recently and industrially polluted. That is, CO was >80 ppb, and the hydrocarbon-ratio figures indicated lesser ages (1.3×10^{-3} and 2.5). Furthermore, the plume that followed the trajectory path was not influenced by convection over Asia. This attribution is an instance of a plausible general phenomenon, where subtrop-
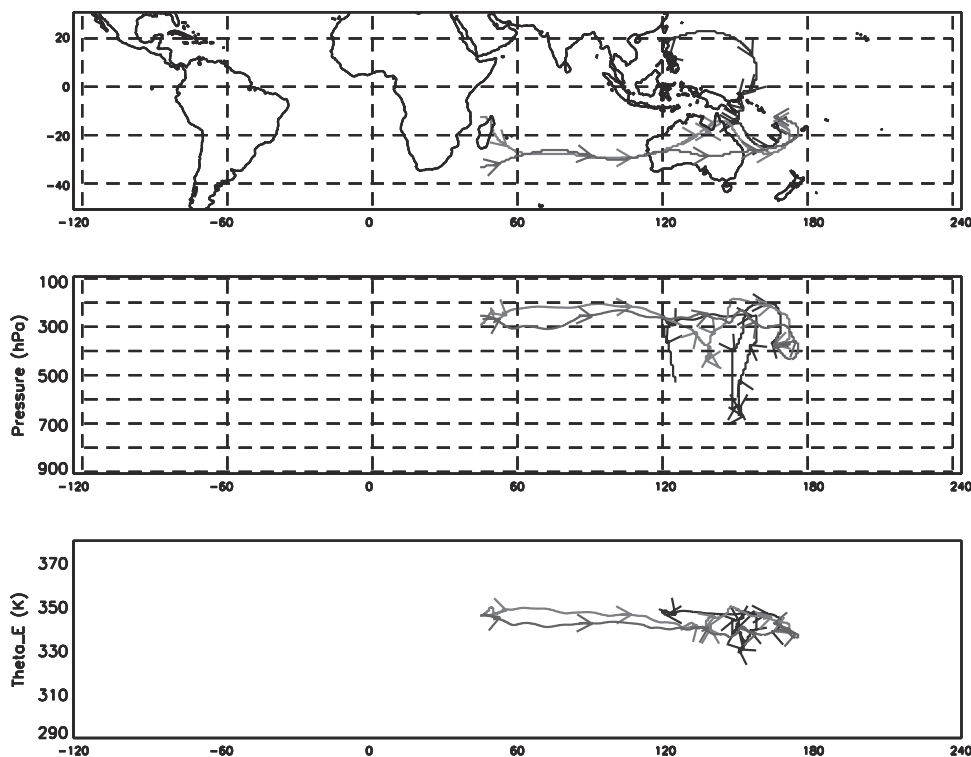
Figure 9. Trajectories suggesting that the CO shown in Figure 8 did originate from Madagascar or points east. Trajectories at higher levels exhibiting high CO indicated more likely origins in southeast Asia or Indonesia, while the lower levels had complex histories, with possible northern hemisphere influence.

Figure 10. (a) Similar map of CO 8 km on 16 March 1999, showing several northern subtropical plumes extending from South America, Africa, and perhaps South Asia at a high point in the Northern Hemisphere spring burning season. Track of the P3B aircraft is below the 8-km level. The flight pattern by the DC-8 at through this time is marked: green indicates within 2 km of the map. (b) Back-trajectory calculations made from the 8.2-km level at the approximate DC-8 position. No cloud lofting was simulated along these paths over Asia, though some trajectories encountered light convection as they passed through the meridian, ~160°E in the Pacific. The trajectories and maps that suggest the possibility that the southern portions of the Northern Hemispheric CO maximum (light green, >75 ppb CO) could be influenced by northern subtropical plume stranding together with broader patterns of Northern Hemisphere pollution. Strands of the subtropical plume appear clearer over Asia.

ical (largely burning-origin) plumes interweave at the southern borders of the Northern Hemisphere cap of generalized CO pollution.

[59]   We do not know of any periods when plumes sampled in the PEM-Tropics B or other GTE expeditions have been given this attribution. They may be sampled in the upcoming GTE mission off the coast of East Asia called TRACE-P. Such influences would only be suggested by simulations that could pinpoint origins, e.g., tracer simulations with very little numerical diffusion.

[60]   There are similarities of this subtropical plume to the southern global plume: (1) an origin in a pollution-accumulating subtropical region (Africa), with its seasonal burning maximum close to the spring equinox before the summer rains; (2) transmission or ducting through the equinoctal

Indian Ocean region, without strong effects of monsoon circulations of the extreme season; and (3) transport in the rapid winds unbroken by storm circulatins of the subtropical jet region.

3.6. Statistical Comparisons of Observations and Simulation

[61]   Some of the tentative observations we have made about strength and positions of modeled plumes can be given more general support using statistics of all the South Pacific flights. Additionally, our model statistics can help show that the observations made by the DC-8 were relatively typical. Figure 11 shows comparisons of the CO observed during the DC-8 flights made in the South Pacific and our simulation of the biomass-burning CO tracer.
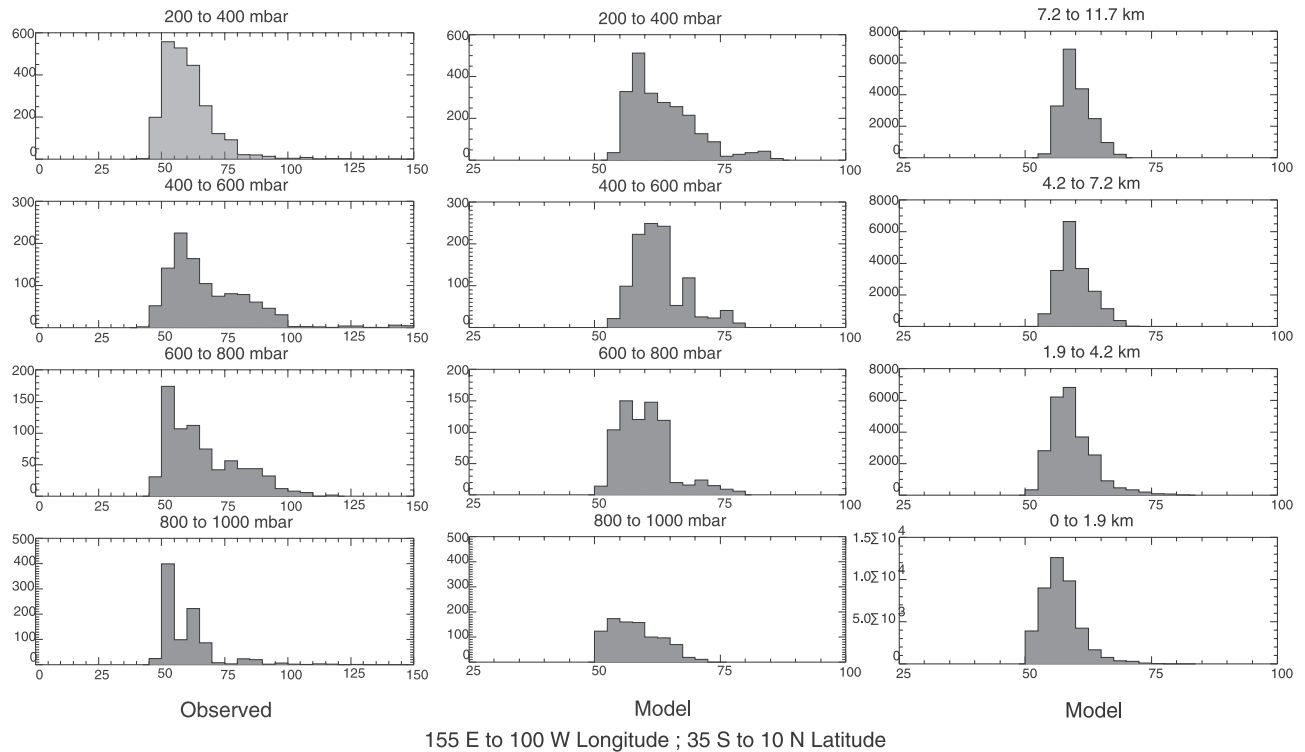
Figure 11. Histograms showing the relative frequency of occurrence of carbon monoxide in the South Pacific, as shown by different sampling strategies. Histograms are shown by four altitude layers, each essentially representing 1/4 of the tropospheric mass below 12 km. The sampling area is indicated, from 155°E near New Zealand to 100°W, including Easter Island. (a) CO (in parts per billion) sampled along the DC-8 flight tracks made in the area as measured by the Sachse differential absorption CO measurement (DACOM) instrument on board. (b) CO tracer from our model, as sampled along the same DC-8 flight track. Note different scale. (c) CO tracer as sampled throughout the entire model volume. Note the differing number of samples but general similarity in distribution shape to the observations. Note that high concentrations are truncated.

Histograms present the number of incidences of CO in each of four different layers of the atmosphere. The layers are defined by pressure so as to weight equally layers of equal masses for whole South Pacific between 10°N and 35°S. There are three columns in Figure 11. The left column shows the histogram of observed CO along the aircraft flight tracks, as measured by the Sachse NASA Langley group. The middle column shows samples from the model along the same flight tracks and the same times, figuratively flying the plane through the model results. The transport simulation used for this analysis uses the *Walcek* [1999] transport scheme. Each of these histograms has relatively few incidences since the aircraft can sample on a miniscule portion of the troposphere. A relatively coarse temporal sampling interval was used since the number of "separate instances," for statistical purposes, is not determined by the CO instrument, which has little random instrumental error, but rather by the number of "different air parcels sampled," i.e., a number restricted by the autocorrelation of the CO measurement series. The right-hand column contains all of the simulated data for the period from the complete domain indicated and thus many more "air parcels."

[62] Table 1 gives the statistics of the left and central histogram sets, that is, it compares the observed CO and modeled tracer-CO sampled along the flight path. The obser-

vations show both more low concentrations (<50 ppb) and high concentrations (>80 ppb) than the model does. There seem to be different effects at work here. The low observed concentrations, almost all 45–50 ppb, might be attributed to

Table 1. Statistics for Observed and Simulated CO[a]

	Observations	Model
200–400 hPa, MD[b] *9.5*		
Median	58.3	64.8
Mean	60.7	67.6
Standard Deviation	11.6	9.8
400–600 hPa, MD 12.2		
Median	64.4	65.4
Mean	69.8	67.4
Standard Deviation	20.6	6.7
600–800 hPa, MD 11.2		
Median	62.3	63.4
Mean	66.4	64.9
Standard Deviation	14.4	6.6
800–1000 hPa, MD 8.6		
Median	56.3	61.3
Mean	60.1	62.0
Standard Deviation	11.6	6.2

[a]Values given in parts per billion.
[b]MD denotes mean absolute deviation of model from observations.

our inexact description of the boundary condition and our neglect of CO oxidation. There could also be stratospheric influences, and our model was not carefully constructed to simulate stratosphere-to-troposphere exchange. Still the observations seem to indicate that major effects of stratospheric exchange are not frequently seen in the troposphere by depression of CO toward 25 ppb or less. This provides a somewhat different viewpoint from that provided by the incidence of high ozone and low water vapor. High ozone and low water vapor may also indicate tropospheric ozone deriving from clouds venting to the uppermost troposphere.

[63] The model gives many more low-peak mixing ratios for CO, especially in the lower midtroposphere. Table 1 describes the model behavior more quantitatively. The median concentrations agree well. This is partly by construction (e.g., the assumed 50-ppb background concentrations which flow in from the north and south boundaries) and partly to skill in simulation of sources and transport. The mean concentrations differ more, and the variance of the observations is twice that of the simulations in the uppermost and lower middle troposphere and >5 times as great in the upper middle troposphere. Some thoughts on the lack of variability come in section 3.7.

[64] Now compare all three histograms. Clearly, there appears to be sampling variation for the distribution of CO in both sets using sample points along the flight tracks. Each pair of histograms shows similarities. Normally, one would expect that sampling from the simulation along the flight path would provide a better match to meteorological conditions, and some similarities of the left and central histograms might be explained this way. Consider, however, the lower troposphere, from 600–800 hPa, for a differing example. The right histogram, for the whole domain, shows a larger proportion of "plumes" above 75 ppb than the does the middle histogram, which is sampled along the flight path. Could this mean that the concentrations sampled along the flight path happened to contain relatively many "near misses"? We suspect not, but rather that the simulation area exhibited an east-west bias and that plumes were in the larger model domain. Perhaps lower plumes were characteristically a bit faster (slower) and further east (west) in the simulation. This type of explanation might fit the conditions of Figure 3, where a neighboring model column showed a good-fit profile for lower tropospheric CO. The general point is that we must expect sampling variability in the smaller number of aircraft samples.

[65] Whatever the exact explanations, the general similarity of the three histograms, especially the middle (sampled) and right (all), suggests the following conclusion: The DC-8 may have made a reasonably representative sampling of the equatorial and South Pacific. In particular, the observational sample that the aircraft made did not seem to especially favor meteorological conditions that tend to exhibit plumes. If so, the sampled observations (middle) would be tend to have distinctly higher concentrations than the full-model averages (right).

3.7.   Why Models May Underestimate the Southern Global Plume

[66] Despite the lower mean concentrations and the weaker variability of the simulated tracer CO and despite the likelihood of sampling variability, there are some trends in the forms of the histograms that suggest that the model has some skill. Undoubtedly, numerical diffusion remaining in the model accounts to some extent for the lack of high peak values in the Pacific. Upper tropospheric distributions are more similar, and the model achieves higher values there. We suspect that this is owing to two facts: (1) The trajectories of the parcels are straighter and (2) the parcels have moved more rapidly from their source and been less exposed to numerical diffusion. Perhaps more importantly, uncertainties in the model's calculated anisentropic motions are smaller for these parcels: The parcels remain either above the region of maximum radiative cooling, which the model may underestimate, or the radiation has had less time to act. The previous case studies illustrate our evidence below that the important sources of the carbon monoxide are from surface burning emissions in Africa and South America.

[67] How well did we do in the simulation of the source region? Figure 12 provides some interesting information. Figure 12 is created by making histograms of concentrations of CO over one important source region, 15°W–45°E longitude and 10°S–40°S latitude. This is roughly the region near southern and central Africa and adjoining oceans on which we reported in a simulation of the TRACE-A experiment. One difference is immediately obvious in the upper two histograms: the choice of 75-ppb boundary conditions in the earlier more limited-area simulation (right histograms). This choice was based on aircraft sampling and may have been most appropriate for that simulation. In our current simulation, represented by the left histograms, a constant 50-ppb concentration was chosen for a more distant southern boundary on the basis of the satellite retrievals by MAPS in 1984 and 1994 rather than aircraft flights in the neighborhood of South Africa [*Chatfield et al.*, 1998]. This might be conservatively low. The model appears to rebuild a large volume of the troposphere around 75 ppb or more on the basis of emissions that are simulated to remain within the regional domain. This may support use of a higher background, especially in the pollution recirculation region of the South Atlantic and adjacent continents.

[68] These effects in simulating the source region may explain the relatively lower variability and low means we see in the Pacific Ocean receptor (measurement) region. Perhaps the paucity of "strong-plume" concentrations simulated at 100–125 ppb (upper left histograms) in our simulation explains the lack of variability. It is true that, despite the 25-ppb offset, the new simulation shows an extended tail of high concentrations >150 ppb in the upper troposphere. This is attributed to somewhat less numerical diffusion in our newer *Walcek* [2000] transport algorithm. However, this tail is not large enough to influence our receptor-region means.

[69] Other effects could be involved. Certainly, we cannot rule out differences in biomass burning between the 2 years, as these might affect upper tropospheric CO concentrations. *Olson et al.* [1999] point out that areas of South Africa may have had fires with larger fuel supplies. *Staudt et al.* [2001] point out that the TOMS absorbing aerosol concentration indices associated with Africa were not unusual high levels in 1996, although periods leading to the "megaplume" of

TRACE-A Africa-Ocean Region
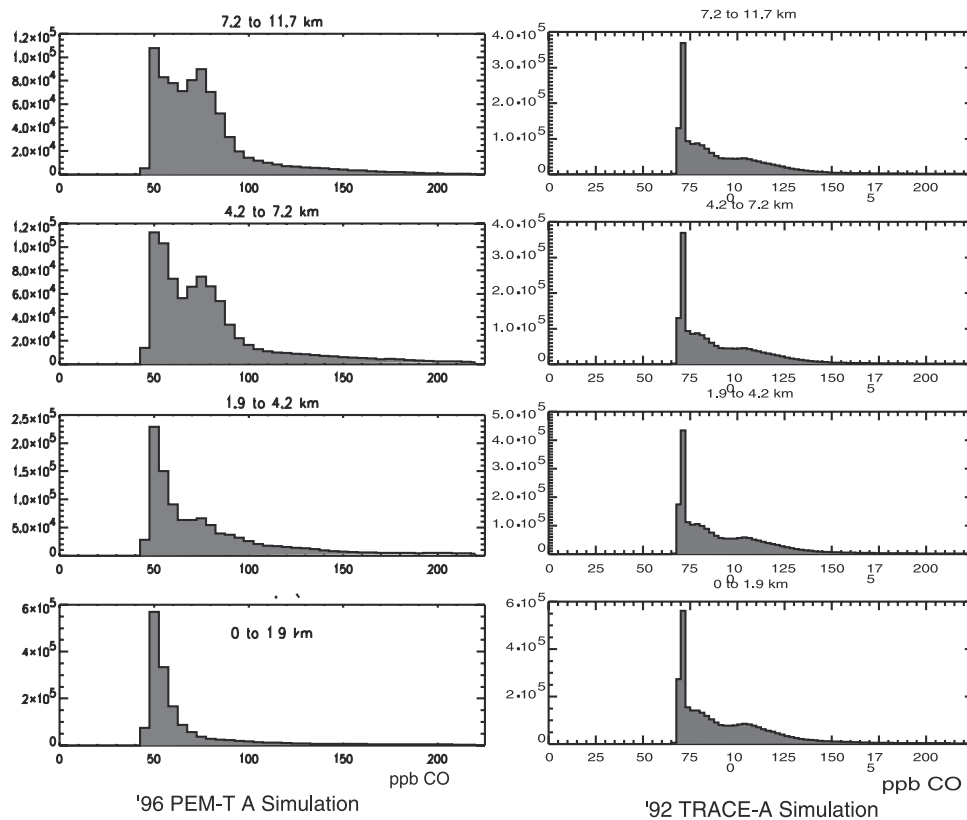
Figure 12. Histogram of simulated CO tracer in an eastern portion of the TRACE-A region. Sampling was in a region generally similar to that shown in Figure 8 of *Chatfield et al.* [1998], but sampling in the cited figure is along TRACE-A flight routes only. On the left are simulations using the meteorology and 100-km grid resolution for 1996 (PEM-Tropics A period), and on the right are simulations using the meteorology and 110-km grid resolution used for 1992 [*Chatfield et al.*, 1998]. Simulations for the September–October 1996 period tend to be lower throughout the troposphere. In part, this results from the boundary conditions used. Other possible reasons for the lower spread of concentrations are discussed in section 3.7.

18 and 24 September exhibited high values. We used the same climatological estimates of carbon burning and CO emissions for both models, so this should not affect differences in our simulations of CO. We have not made an analysis to rule out other differences in simulation, such as differing convective weather in the two years 1992 (TRACE-A) and 1996 (PEM-Tropics A). Staudt et al. (submitted manuscript, 2002) describe such an explanation, e.g., more direct transport patterns east of Africa due to stronger jets.

4. Summary

4.1. Catalog of Global Pollution Features

[70] Characteristic pollution features that we find, using simulated and observed carbon monoxide as a guide [see also *Allen et al.*, 1996; *Bey et al.*, 2001; *Holloway et al.*, 2000; Staudt et al., submitted manuscript, 2002], might be named the following: (1) a northern pollution "vortex" containing an admixture of three major pollution plumes from America, Europe, and East Asia spreading around the world; (2) equatorial plumes extending ~2000 km east of equatorial Africa (the Great African plume) but also from

South America and sometimes Indonesia; (3) subtropical global plumes, including the plume whose fragments were encountered in PEM-Tropics A, up to ~20,000 km downwind. This paper has illustrated a southern global plume ~15°–30°S. *Chatfield et al.* [1998] indicated that Africa can alternate its export pattern to an equatorial plume and what we now call the southern global plume. There is also a northern counterpart that may strand into the northern pollution vortex.

4.2. Conclusions

[71] We have illustrated a mechanism that conducts air pollution to the South Pacific from sources predominantly in central Africa and South America in austral spring. This southern global plume is the most important instance of a more generic feature, a subtropical global plume. A frequently occurring sequence of events elaborated in the introduction has been illustrated with two case studies. Our general impression of the entire PEM-Tropics A period is that it is similar to the case studies, with some variation noted below. We find (1) a pattern of continental accumulation, (2) characteristic convergence and divergence asso-

ciated with each continent associated with cumulonimbus convection or synoptic storms, (3) a tendency toward intercontinental accumulation and plume merging near the source region, with (4) often a final pollutant injection by cloud convection over southern Africa. Quite frequently, there is (5) a pattern of undulating but rapid undilute transport across the South Indian Ocean and Australia, (6) subsidence of the plumes by both isentropic and diabatic, radiative processes, especially <9 km. Finally, there is (7) increasing undulation, splintering, and likelihood of dispersion in the Pacific.

[72] We must be clear that other patterns of transport occur. We found in our simulation, also isolated, incidences of two other pollution patterns. A few low-lying plumes below 4 km seemed to trace back to nearby Australia. Additionally, there were instances in which plumes from Southeast Asia would drift westward across the Indian Ocean, perhaps reaching Africa. They would then recurve and join the general pollutant flow. *Board et al.* [1999] describe this source region more fully and find instances of trajectories recurving as far east as the region south of the Bay of Bengal. Though the illustrated trajectories do not show this, our trajectories tend to have more daily alteration in course than do the *Board et al.* [1999] trajectories since they are based on assimilated hourly wind data.

[73] These points address question (3) of our introduction on the mechanism of transport. Other questions were also posed and can be only partially answered. (1) The statistics of simulated CO tracer in the South Pacific and the sample that was cut by the DC-8 flight path differed but not to a great degree. Though simulations and observations disagreed significantly in magnitude, it does not appear that the DC-8 aircraft sampling of the Pacific was strongly biased to samples of the southern global plume. (2) The plume was perhaps somewhat more strongly directed than in other years, as *Staudt et al.* [2001] and Staudt et al. (submitted manuscript, 2002) have argued. Nevertheless, the typical values shown by the histograms in Figure 11 are close in magnitude to the MAPS midtropospheric CO estimates of 1984 and lower than those of 1994. *Pratt and Falconer's* [1979] values are generally similar to the few early samples of GASP in 1977. *Pratt and Falconer's* [1979] quotation of mean African and Pacific CO averages (89 and 66 ppb) seem amazingly close to the observations summarized in Figures 11 and 12 and in Table 1. So perhaps the CO climatology of October 1999 was somewhat elevated, with one exceptional outbreak, but was not greatly untypical.

[74] What happens to the southern global plume when biomass burning is not so active? Some plumes persist, as we have seen in Figure 7. We may expect that several patterns of trace gas spread seen in this paper will apply. A plume of somewhat elevated CO may also be expected; partially from biomass burning and partially from vegetative emissions [*Zimmerman et al.*, 1978]. To the extent that lightning influenced both TRACE-A and PEM-Tropics A NO_x [*Smyth et al.*, 1996] a southern global plume is presumably a permanent source of nitrogen oxides and ozone generation for the free troposphere of the Southern Hemisphere [see *Schultz et al.*, 1999]. In other seasons we may expect that the position of the subtropical jets and the storm track in Indian and Pacific Oceans will alter the predominant latitudes of influence. This explanation works well for the example we showed in Figure 7 with limited penetration into the Pacific Basin due to more disturbed weather and storminess, e.g., more complex and diffusive transport patterns all along the way. Nevertheless, subtropical free-tropospheric maxima of trace gases may be expected.

[75] We can make some tentative suggestions that could help improve simulation of the subtropical global plume and other long-distance transport. We suspect that the weak variation of CO tracer in our model was due to several causes that may be improved in more complex models. First, a higher boundary condition for the source region might have been appropriate and magnified the plumes that reached the cleaner Pacific region. Remaining numerical diffusion could lower the peaks. The strength of the parameterized convective mass flux might also reasonably be larger. We expect all such parameterizations will need careful checking with tracer simulations; as seen by *Chatfield et al.* [1998], CO seems to provide a very good test tracer. There is some evidence that plumes were carried by the model to the Pacific but tended to subside to regions away the path of DC-8 sampling. This could be a chronic difficulty with shear and subsidence over long time periods. Small errors in reconstructing the vertical wind shear, or integrating its transport effects upon CO, would be magnified greatly over tens of thousands of kilometers.

References

Allen, D. J., P. Kasibhatla, A. M. Thompson, R. B. Rood, B. G. Doddridge, K. B. Pickering, R. Hudson, and S.-J. Lin, Transport-induced interannual variablity of carbon monoxide determined using a chemistry and transport model, *J. Geophys. Res.*, *101*, 28,655–28,670, 1996.

Arakawa, A., and V. R. Lamb, Computational design of the basic dynamical processes of the UCLA general circulation model, in *Methods in Computational Physics*, vol. 17, pp. 174–265, Academic, San Diego, Calif., 1977.

Arakawa, A., and W. H. Schubert, Interaction of a cumulus cloud ensemble with the large scale environment, part I, *J. Atmos. Sci.*, *31*, 674–701, 1974.

Bey, I., D. J. Jacob, J. A. Logan, and R. M. Yantosca, Asian chemical outflow to the Pacific in spring: Origins, pathways, and budgets, *J. Geophys. Res.*, *106*, 23,097–23,114, 2001.

Board, A. S., H. E. Fuelberg, G. L. Gregory, B. G. Heikes, M. G. Schultz, D. R. Blake, J. E. Dibb, S. T. Sandholm, and R. W. Talbot, Chemical characteristics of air from differing source regions during the Pacific Exploratory Mission-Tropics A (PEM-Tropics A), *J. Geophys. Res.*, *104*, 16,181–16,196, 1999.

Brasseur, G., D. Hauglustaine, and S. Walters, Chemical compounds in the remote Pacific troposphere: Comparison between MLOPEX measurements and chemical transport model calculations, *J. Geophys. Res.*, *101*, 14,795–14,813, 1996.

Chatfield, R. B., and A. C. Delany, Convection links biomass burning to increased tropical ozone; however, models will tend to overpredict O_3, *J. Geophys. Res.*, *95*, 18,473–18,488, 1990.

Chatfield, R. B., J. A. Vastano, H. B. Singh, and G. W. Sachse, A general model of how fire emissions and chemistry produce African/oceanic plumes (O3, CO, PAN, smoke) in TRACE A, *J. Geophys. Res.*, *101*, 24,279–24,306, 1996.

Chatfield, R. B., J. A. Vastano, L. Li, G. W. Sachse, and V. S. Connors, The Great African plume from biomass burning: A three-dimensional study of TRACE A carbon monoxide, *J. Geophys. Res.*, *103*, 28,059–28,077, 1998.

Crutzen, P. J., and L. T. Gidel, A two-dimensional photochemical model of

the atmosphere, 2, The tropospheric budgets of the anthropogenic chlorocarbons, CO, CH₄, CH₃Cl, and the effect of various NOₓ sources on tropospheric ozone, *J. Geophys. Res.*, 88, 6641–6661, 1983.

Crutzen, P. J., and P. H. Zimmermann, The changing photochemistry of the troposphere, *Tellus, Ser. A/B*, 43, 136–151, 1991.

Crutzen, P. J., L. E. Heidt, J. P. Krasneck, W. H. Pollock, and W. Seiler, Biomass burning as a source of atmospheric trace gases: CO, H₂, N₂O, NO, CH₃Cl and COS, *Nature*, 282, 253–256, 1979.

Dickerson, R. R., et al., Thunderstorms: An important mechanism in the transport of air pollutants, *Science*, 95, 460–465, 1987.

Fishman, J., K. Fakhruzzaman, B. Cros, and D. Nganga, Identification of widespread pollution in the Southern Hemisphere deduced from satellite analyses, *Science*, 252, 1693–1696, 1991.

Fuelberg, H. E., R. E. Newell, S. P. Longmore, Y. Zhu, D. J. Westberg, E. V. Browell, D. R. Blake, G. R. Gregory, and G. W. Sachse, A meteorological overview of the Pacific Exploratory Mission (PEM) Tropics period, *J. Geophys. Res.*, 104, 5585–5622, 1999.

Galanter, M., H. Levy II, and G. R. Carmichael, Impacts of biomass burning on tropospheric CO, NOₓ, and O₃, *J. Geophys. Res.*, 105, 6633–6653, 2000.

Granier, C., J.-F. Müller, S. Madronich, and G. Brasseur, Possible causes for the decrease in the 1990–1993 global tropospheric CO abundances: A three-dimensional sensitivity study, *Atmos. Environ.*, 30, 1673–1682, 1996.

Grell, G. A., Prognostic evaluation of assumptions used by cumulus parameterizations, *Mon. Weather Rev.*, 121, 764–787, 1993.

Grell, G. A., J. Dudhia, and D. Stauffer, A description of the fifth-generation Penn State/NCAR Mesoscale Model (MM5) NCAR/TN-398+STR, Univ. Corp. for Atmos. Res., Boulder, Colo., 1995.

Hauglustaine, D. A., G. P. Brasseur, S. Walters, P. J. Rasch, J.-F. Muller, L. K. Emmons, and M. A. Carroll, MOZART: A global chemical transport model for ozone and related chemical tracers, 2, Model results and evaluation, *J. Geophys. Res.*, 103, 28,291–28,336, 1998.

Heidt, L. E., J. P. Krasnec, R. A. Lueb, W. H. Pollock, B. E. Henry, and P. J. Crutzen, Carbon monoxide, *J. Geophys. Res.*, 85, 7329–7336, 1980.

Hoell, J. M., D. D. Davis, D. J. Jacob, M. O. Rodgers, R. E. Newell, H. E. Fuelberg, R. J. McNeal, J. L. Raper, and R. J. Bendura, Pacific Exploratory Mission in the tropical Pacific: PEM-Tropics A, August–September 1996, *J. Geophys. Res.*, 104, 5567–5583, 1999.

Holloway, T., H. Levy, and P. S. Kasibhatla, Global distribution of carbon monoxide, *J. Geophys. Res.*, 105, 12,123–12,147, 2000.

Hong, S.-Y., and H.-L. Pan, Nonlocal boundary layer vertical diffusion in a medium-range forecast model, *Mon. Weather Rev.*, 124, 2322–2339, 1996.

Jenkins, G. S., K. Mohr, V. R. Morris, and O. Arino, The role of convective processes over the Zaire-Congo Basin to the southern hemisphere ozone maximum, *J. Geophys. Res.*, 102, 18,963–18,980, 1997.

Kuo, Y.-H., J. R. Gyakum, and Z. Guo, A case of rapid continental mesoscale cyclogenesis, part 1, Model sensitivity experience, *Mon. Weather Rev.*, 123, 970–997, 1995.

Kwok, H. C., W. E. Langlois, and R. A. Ellefsen, Digital simulation of the global transport of carbon monoxide, *IBM J. Res. Develop.*, 15, 3–9, 1971.

Logan, J. A., and V. W. J. H. Kirchoff, Seasonal variation of tropospheric ozone at Natal, Brazil, *J. Geophys. Res.*, 91, 7875–7881, 1986.

Logan, J. A., M. J. Prather, S. C. Wofsy, and M. B. McElroy, Tropospheric chemistry: A global perspective, *J. Geophys. Res.*, 86, 7210–7254, 1981.

Olson, J. R., B. A. Baum, D. R. Cahoon, and J. H. Crawford, Frequency and distribution of forest, savanna, and crop fires over tropical regions during PEM-Tropics A, *J. Geophys. Res.*, 104, 5865–5876, 1999.

Peters, L., and A. A. Jouvanis, Numerical solution of the transport and chemistry of CH₄ and CO in the atmosphere, *Atmos. Environ.*, 13, 1443–1462, 1979.

Pickering, K. E., et al., Convective transport of biomass burning emissions over Brazil during TRACE-A, *J. Geophys. Res.*, 101, 23,993–24,012, 1996a.

Pickering, K. E., A. M. Thompson, D. P. McNamara, M. R. Schoeberl, H. E.

Fuelberg, R. O. Loring Jr., M. V. Watson, K. Fakhruzzaman, and A. S. Bachmeier, TRACE-A trajectory intercomparison, 1, Effects of different input analyses, *J. Geophys. Res.*, 101, 23,909–23,926, 1996b.

Pinto, J. P., Y. L. Yung, D. Rind, L. Russel, J. A. Lerner, J. E. Hansen, and S. Hameed, A general circulation model study of atmospheric carbon monoxide, *J. Geophys. Res.*, 88, 3691–3702, 1983.

Potter, C. S., J. T. Randerson, C. B. Field, P. A. Matson, P. M. Vitousek, H. A. Mooney, and S. A. Klooster, Terrestrial ecosystem production: A process model based on global satellite and surface data, *Global Biogeochem. Cycles.*, 7, 811–841, 1993.

Pougatchev, N. S., G. W. Sachse, H. E. Fuelberg, C. P. Rinsland, R. B. Chatfield, V. S. Connors, N. B. Jones, J. Notholt, P. C. Novelli, and H. G. Reichle Jr., Pacific Exploratory Mission-Tropics carbon monoxide measurements in historical context, *J. Geophys. Res.*, 104, 26,195–26,208, 1999.

Pratt, R. W., and P. Falconer, Circumpolar measurements of ozone, particles, and carbon monoxide from a commercial airliner, *J. Geophys. Res.*, 84, 7876–7882, 1979.

Roelofs, G.-J., J. Lelieveld, and R. van Dorland, A three-dimensional chemistry/general circulation model simulation of anthropogenically derived ozone in the troposphere and its radiative climate forcing, *J. Geophys. Res.*, 102, 23,389–23,403, 1997.

Scala, J. R., M. Garstang, T. Wei-Kuo, K. E. Pickering, A. M. Thompson, J. Simpson, V. W. J. H. Kirchoff, E. V. Browell, and G. Sachse, Cloud-draft structure and trace-gas transport, *J. Geophys. Res.*, 95, 17,015–17,030, 1990.

Schultz, M., et al., The origin of tropospheric ozone and NOₓ over the tropical South Pacific, *J. Geophys. Res.*, 104, 5829–5844, 1999.

Selier, W., The cycle of atmosphere CO, *Tellus*, 26, 117–135, 1974.

Selier, W., and P. J. Crutzen, Estimates of gross and net fluxes of carbon between the biosphere and the atmosphere from biomass burning, *Clim. Change*, 2, 204–247, 1980.

Smolarkiewicz, P., and W. W. Grabowski, The multidimensional positive definite advection transport algorithm: Non-oscillatory option, *J. Comp. Phys.*, 86, 355–375, 1990.

Smyth, S., et al., Factors influencing the upper free tropospheric distribution of reactive nitrogen over the south Atlantic during the TRACE-A experiment, *J. Geophys. Res.*, 101, 24,165–24,186, 1996.

Staudt, A. C., D. J. Jacob, J. A. Logan, D. Bachiochi, T. N. Krishnamurti, and G. W. Sachse, Continental sources, transoceanic transport, and interhemispheric exchange of carbon monoxide over the Pacific, *J. Geophys. Res.*, 106, 32,571–32,590, 2001.

Torres, O., P. K. Bhartia, J. R. Herman, Z. Ahmad, and J. Gleason, Derivation of aerosol properties from satellite measurements of backscattered ultraviolet radiation: Theoretical basis, *J. Geophys. Res.*, 103, 17,099–17,110, 1998.

van Leer, B., Toward the ultimate conservative difference scheme, IV, A new approach in numerical convection, *J. Comput. Phys.*, 23, 276–299, 1977.

Walcek, C., Minor flux adjustment near mixing ratio extremes for simplified yet highly accurate monotonic calculation of tracer advection, *J. Geophys. Res.*, 105, 9335–9348, 2000.

Zimmerman, P. R., R. B. Chatfield, J. Fishman, P. J. Crutzen, and P. L. Hanst, Estimates of the production of CO and H₂ from the oxidation of hydrocarbon emissions from vegetation, *Geophys. Res. Lett.*, 5, 679–682, 1978.

————————

D. R. Blake and N. J. Blake, Department of Chemistry, 516 Rowland Hall, University of California, Irvine, CA 92697-2025, USA. (drblake@uci.edu; nblake@uci.edu)

R. B. Chatfield and G. W. Sachse, Earth Science Division, NASA Ames Research Center, Moffett Field, CA 94035-1000, USA. (chatfield@clio.arc.nasa.gov)

Z. Guo, WNI Oceanroutes, 333 W. El Camino Real, Suite 300, Sunnyvale, CA 94087, USA. (zguo@wni.com)